Mechanistic understanding of catalytic transformations

Dissertation for the degree of Doctor Philosophiae

Santeri Aikonen
University of Helsinki
Faculty of Science
Department of Chemistry
P.O. Box 55 (A.I. Virtasen aukio 1)
FI-00014 University of Helsinki, Finland

To be presented, with the permission of the Faculty of Science, University of Helsinki, for public discussion in Auditorium A129, Department of Chemistry (A.I. Virtasen aukio 1, Helsinki), on November 25, 2020, at noon.

Helsinki 2020

Supervised by

Dr. Juho Helaja
Department of Chemistry
University of Helsinki
Helsinki, Finland

Dr. Mikko Muuronen
Current affiliation: BASF SE
Ludwigshafen, Germany

Reviewed by

Prof. Ville R. I. Kaila
Department of Biochemistry and Biophysics
Stockholm University
Stockholm, Sweden

Dr. Michael Patzschke
Institute for Resource Ecology
Department of Chemistry of the f-elements
Helmholtz-Zentrum Dresden-Rossendorf
Dresden, Germany

Opponent

Prof. Feliu Maseras
Institute of Chemical Research of Catalonia
Departament de Química
Universitat Autònoma de Barcelona
Barcelona, Spain

ISBN 978-951-51-6806-1 (paperback)
ISBN 978-951-51-6807-8 (PDF)
http://ethesis.helsinki.fi
Unigrafia Helsinki 2020

All models are wrong, but some are useful.

George E. P. Box

Abstract

Reaction mechanisms play an integral part in understanding chemical phenomena. Chemists use their knowledge of reaction mechanisms both when formulating research questions and when carrying out experiments in the fume hood or *in silico*. Accurate understanding of the reaction mechanism provides a pre-requisite for optimisation of reaction conditions or development of new catalysts. Reaction mechanisms are studied with experimental, *e.g.*, *in situ* reaction monitoring or isotopic labelling, and computational methods as the mechanistic findings complement each other.

This work combined experimental, kinetic analysis and computational methods to elucidate reaction mechanisms in homogeneous gold-catalytic activations of alkynes, photoreduction reactions of heteroaryls and oxidative coupling reactions of (hetero)aryls. Computational methods are in a central role for mechanistic explorations, and a part of this thesis is dedicated for the review of the central theory of these methods. Central mechanistic aspects of the studied reactions are also presented. The experimental and computational results presented in this thesis have been published in three peer-reviewed publications; and two manuscripts are under preparation for submission.

In Publication I, we discovered the reaction mechanism of gold(I)-catalysed intermolecular 1,3-*O*-transposition of ynones using kinetic analysis and experimental and computational methods. We then optimised the conditions with aldehyde additives and introduced a prediction model based on the aldehydes' nucleophilicities.

In Publication II, we studied the proton and electron transfer steps in the $Ru(bpy)_3Cl_2$ and ascorbic acid-mediated photoreduction of N-heterocyclic nitroaryls to N-heterocyclic amines. From computational thermodynamics and experimental kinetics, we concluded that the first reduction is a multisite proton-coupled electron transfer while the last reduction is a stepwise protonation and electron transfer.

In Publications III and IV, we studied the oxidative dehydrogenative C-C coupling mechanisms, *i.e.*, radical cation and arenium cation, in heterogeneous carbocatalysis. We concluded that both mechanisms are kinetically feasible in the reaction conditions and the operative mechanism depends on the proton and electron affinities of the substrate and the catalyst.

In Publication V, we developed hydrogen bond donor tethered ligands for gold(I)-catalysis. The side-arms activated the gold-chloride bond with the help of hydrogen bond donating substrates or additives, as well as energetically stabilised reaction intermediates and transition states. The developed catalysts proved to be superior compared to commercial gold(I)-catalysts in oxazoline cycloisomerisation.

In all Publications, the combination of experimental and computational mechanistic explorations offered insight into the reactions that would have otherwise been difficult to attain. The experimental and computational methods were used to optimise reaction conditions and predict reactivity based on simple chemical descriptors, such as acidity, redox potential and nucleophilicity.

List of Publications

Publications and manuscripts representing the results of this work:

I. **S. Aikonen**, M. Muuronen,* T. Wirtanen, S. Heikkinen, J. Musgreave, J. Burés,* J. Helaja,* Gold(I)-Catalyzed 1,3-*O*-Transposition of Ynones: Mechanism and Catalytic Acceleration with Electron-Rich Aldehydes, *ACS Catalysis* **2018**, *8*, 960–967.

II. A. R. Todorov, **S. Aikonen**, M. Muuronen, J. Helaja,* Visible-Light Photocatalyzed Reductions of N-heterocyclic Nitroaryls to anilines utilizing ascorbic acid reductant, *Organic Letters* **2019**, *21*, 3764–3768.

III. T. Wirtanen, **S. Aikonen**, M. Muuronen, M. Melchionna, M. Kemell, F. Davodi, T. Kallio, T. Hu, J. Helaja,* Carbocatalytic Oxidative Dehydrogenative Couplings of (Hetero)Aryls by Oxidized Multi-Walled Carbon Nanotubes in Liquid Phase, *Chemistry – A European Journal* **2019**, *25*, 12288–12293.

IV. D. S. Casadio,† **S. Aikonen**,† A. Lenarda, M. Nieger, T. Hu, S. Taubert, D. Sundholm, M. Muuronen, T. Wirtanen, J. Helaja,* Divergent Carbocatalytic Routes in Oxidative Coupling of Benzofused Heteroaryl Dimers: A Mechanistic Update, *Manuscript*

V. O. Seppänen,† **S. Aikonen**,† M. Muuronen, C. Alamillo-Ferrer, J. Burés, J. Helaja,* Dual H-bond activation of NHC-Au(I)-Cl complexes with amide functionalized side-arms assisted by H-bond donor substrates or acid additives, *Manuscript*

† Shared first author * Corresponding author

Author contributions

I. The author performed all experimental and computational work. J.M. and J.B. performed the kinetic analysis and S.H. helped with NMR-experiments. M.M., T.W. and J.H. supervised the work. The manuscript was written with contributions from all authors.

II. The work was divided between the author and A.R.T. for computational and experimental work, respectively. M.M. and J.H. supervised the work. The manuscript was written with contributions from all authors.

III. The work was divided between the author and T.W. for computational and experimental work, respectively. M.K. measured XRD and M.M. measured PET of the material. F.D. and T.K. measured the CV spectra of nanotubes. T.H. performed XPS-analysis of the material. M.M. and J.H. supervised the work. The manuscript was written with contributions from all authors.

IV. The work was divided equally between the author and D.S.C. for computational and experimental work, respectively. A.L. performed CV-measurements, M.N. performed X-ray analysis and T.H. performed XPS-analysis of the material. S.T. computed the ring-currents and T.W. simulated the ECD spectrum with help of D.S. M.M and J.H. supervised the work. The manuscript was written with contributions from all authors.

V. The work was divided equally between the author and O.S. for computational and experimental work, respectively. C.A.-F. and J.B. performed the kinetic analysis. M.M. and J.H. supervised the work. The manuscript was written with contributions from all authors.

The author wrote the mechanistic part for all manuscripts.

Acknowledgements

I want to express my gratitude to my supervisors: Dr. Juho Helaja and Dr. Mikko Muuronen. Juho, for the past five years I have wandered every day into your office and spent countless hours discussing chemistry, no matter how late the hour was. You have challenged my ideas and given me your full support and freedom to work on different research projects. Mikko, even when you were in the middle of the Amazon rainforest, you found the time to help me to solve my problems. We have discussed everything from chemistry and career choices to life in general. You have taught me everything I know about quantum chemistry and encouraged me to go even further. I thank both of you for your time and shared knowledge.

I am grateful to Prof. Ville R. I. Kaila and Dr. Michael Patzschke for reviewing my thesis and providing such excellent comments and feedback. I would like to acknowledge Prof. Feliu Maseras for being the opponent for the dissertation of this thesis. I also want to thank Prof. Timo Repo for acting as the custos of the defense and for all the insightful discussion we have had.

I have had the pleasure to share all of my publications with co-authors from the group: Tom, Aleksandar, Otto, David, and Anna, thank you for all the discussions, friendship and co-authoring the articles. I want to also thank all the past and present group members who I have had the pleasure to work and interact with: Aleksandar, Anna, David, Erika, Evgeny, Florian, Iida, Ina, Juho (Koivula), Juulia, Kiia, Lukas, Mikko (Muuronen), Mikko (Mäkelä), Otto, Samantha, Shyama, Taru, Tom, and Vladimir. A special thank you goes to students; Emma, Wille, and Yurii, who I have supervised in the lab. I learned a great deal while working with you!

Dr. Jordi Burés from The University of Manchester is greatly acknowledged for his help with the kinetic analysis. I am very grateful to Prof. Robert Paton for hosting my research visit in his group at Colorado State University. Although the trip was cut short due to the COVID-19 outbreak, I learned a great deal during that visit and the group made me feel like home.

I would like to thank Professors Mikko Oivanen, Ilkka Kilpeläinen, Lauri Halonen and Dage Sundholm, in addition to Doctors Jussi Sipilä, Petri Heinonen, Sami Heikkinen, and Stefan Taubert from the Department of Chemistry for

the useful scientific discussions. Dr. Nino Runeberg from the Finnish Centre for Scientific Computing (CSC) is acknowledged for all the technical support. Katja, Marianna, and Valtteri, I value your friendship and support both at work and outside of work. Thank you, Valtteri, for all the lunches we have had together!

I am deeply grateful to the CHEMS doctoral programme for granting me a four-year salaried doctoral student position. The Finnish Cultural Foundation, Alfred Kordelin foundation, and Magnus Ehrnrooth foundation, are also acknowledged. A special thank you to CSC for providing the computational resources for this thesis.

Finally, I want to thank my family for their support during the last thirty years. Especially my grandmother, Anja-mummi; your tireless help with my homework has not gone to waste! My wife's parents, Tanja and Juha, who have given their full support throughout my journey in the academic world. My darling wife, Jenny, without you all of this would be meaningless and I would have not been able to achieve this. My beautiful daughter, Lilian, you are the light of my days and although you do not yet understand any of this I dedicate this book to you.

Santeri Aikonen

Helsinki 2020

Contents

List of Abbreviations

BDFE	bond dissociation free energy
COSMO	conductor-like screening model
COSMO-RS	COSMO for realistic solvation
DCE	1,2-dichloroethane
DCM	dichloromethane
DCSM	dielectric continuum solvation model
DFT	density functional theory
GGA	generalized gradient approximation
GTO	Gaussian-type orbital
HF	Hartree-Fock
HOMO	highest occupied molecular orbital
LUMO	lowest unoccupied molecular orbital
mGGA	meta-GGA
MS-PCET	multi-site PCET
NBO	natural bonding orbital
NHC	N-heterocyclic carbenes
NMR	nuclear magnetic resonance
NPA	natural population analysis
ODH	oxidative dehydrogenative
PCET	proton-coupled electron transfer
RI	resolution-of-identity
RPKA	reaction progress kinetic analysis
SOMO	singly occupied molecular orbital
STO	Slater-type orbital
TTET	triplet-triplet energy transfer
TM	transition-metal
TS	transition state
VTNA	variable time normalization analysis

1. Introduction

Mechanistic understanding forms the core of every chemist's "chemical intuition" that guides the decision making in the laboratory from adaptation of literature protocols to method development. Understanding how the basic concepts of thermodynamics and kinetics relate to reaction mechanisms lays the foundation for our chemical intuition that is acquired during the basic training.

Most contemporary synthetic or catalytic studies include a mechanistic proposal within the article. The mechanism is based on the authors' intuition and is preferably grounded on previous literature, experimental evidence, computational energy profiles, or on a combination of these. However, in some cases, no formal mechanistic proof is presented. The rationale for reaction mechanism is then passed down to subsequent articles, while the mechanistic proposal can go unchallenged for a long time. Mechanistic investigations should, in the writer's opinion, always be carried out as both experimental and computational methods have generally become available and easier to apply for a wide set of chemical problems.

During the last 30 years, computational chemistry and especially density functional theory has undergone a series of developmental steps including the formulation of more accurate and systematic density functionals,[1] inclusion of implicit solvation,[2,3] *ad hoc* addition of dispersion,[4–6] development of perturbed density functional theory,[7] statistical thermodynamics for better solvation,[8,9] and fast *in silico* methods for sampling of chemical space.[10,11] This is in addition to Moore's law and the effect of doubling processor speed every two years. Indeed, computational chemistry and density functional theory has become an integral part of organic chemistry in recent years (see Scheme 1.1, left).

Computational methods are used to calculate Gibbs free energy differences between intermediates and transition states. The computational free energy differences are subsequently used to approximate the equilibrium constants and reaction rates that help to assess whether the reaction is thermodynami-

cally favourable or kinetically feasible. Because it is difficult to acquire Gibbs free energies in condensed-phases, computations should always be connected to experimental results,[12] for example, by comparing the relative reaction rate constants[13] or selectivities[14] to computed activation free energy barriers, or using molecular properties to predict regioselectivity[15,16] and reactivity.[17] One should, however, be aware of the limitations of the contemporary quantum chemical methods. Competing reactions are difficult to predict from computations alone, as it would either require prior knowledge of all possible side reactions or calculation of the complete free energy surface of the whole system, whereas experimental explorations can unambiguously reveal competing reactions.

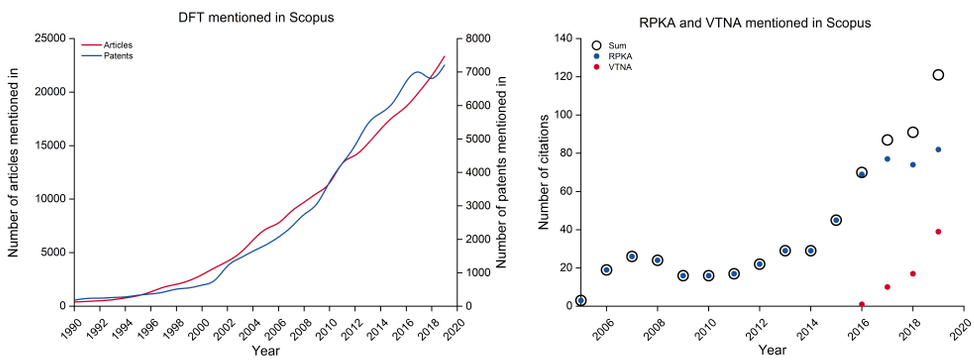

Scheme 1.1. On the left: number of DFT or density functional theory mentions in patents and articles. On the right: number of RPKA or reaction progress kinetic analysis, and VTNA or variable time normalization analysis, mentions in articles.

In the last 20 years, reaction progress kinetic analysis[18,19] and variable time normalization analysis[20,21] have emerged and are steadily gaining popularity (see Scheme 1.1, right). Both methods rely on visual inspection of the reaction kinetics and the results are used to find the rate-determining step and the (experimental) activation free energy. However, determining the driving force of the reaction can be more time consuming in the laboratory, while computational approaches can rationalise the reactivity more effortlessly. Combination of both experimental and computational results provides a powerful methodology for studying reaction mechanisms as they complement each other and can guide further experimentation.

The aim of this work was to study the mechanistic details of gold(I)-catalysed ynone transposition, photoreduction of N-heterocyclic nitroaryls, and carbocatalytic oxidative dehydrogenative C-C coupling of (hetero)aryls. The parallel experimental and computational mechanistic studies offered complementary insight into the reactions and helped to derive mechanistic principles and develop predictive models to rationalise the reactivity with chemical descriptors,

such as $pK_{a(H)}$, E° and nucleophilicity or electrophilicity.

In Publication I, a previously proposed literature reaction mechanism[22,23] contradicted our preliminary computational work and prompted us to carry out mechanistic studies that revealed the literature mechanism to be incorrect. In Publication II, we differentiated between sequential and concerted natures of proton-electron transfers in photoreduction reaction of nitro-N-heterocycles. In Publications III and IV, we proposed that the quinone mediated oxidative dehydrogenative C-C coupling reaction proceeds *via* either radical cation or arenium cation mechanisms, depending on the system. The finding explained central experimental results regarding the reactivity and selectivity, despite heated discussion surrounding the mechanism in the literature.[24,25] Lastly, in Publication V, we studied the unknown activation mechanism of ligated gold(I)-chloride complexes with H-bond tethers in oxazoline cyclisation and enyne cycloisomerisation reactions.

The background of the general chemistry in the studied systems, with focus on the mechanisms and important factors that guide the reactivity, is described in Chapter 2. The computational and experimental methods used in the current work are introduced in Chapter 3. Finally, Chapter 4 contains an overview of the mechanistic findings for each publication and Chapter 5 summarises the current work.

2. Background chemistry

2.1 Homogeneous gold catalysis

In this work, we optimised the reaction conditions of an intermolecular 1,3-*O*-transposition reaction of ynones, and developed bifunctional ligands with hydrogen bond donor-tethered side-arms that were used in activation of L-Au^{I}-Cl complexes. The field of gold catalysis is vast, and, for this reason, the discussion focuses on the mechanistic aspects of homogeneous gold-catalysis.

Gold is a Lewis-acid that can activate π-systems such as alkynes, alkenes, and allenes. For over 20 years, the interest in homogeneous gold-catalysis and its synthetic applications has surged.[26–29] Scalar relativistic effects account for the many attributes of gold(I)-catalysts, such as gold being the most electronegative transition metal (TM) and an efficient activating agent for π-systems.[30] Both Au(I) and Au(III) are tolerant to oxygen and thus gold-catalysis can be carried out under ambient conditions; and gold chemistry is typically not associated with redox reactions like other TMs due to high kinetic barriers for the oxidative addition.[31]

The commonly used gold catalysts include the simple neutral $Au^{I}Cl$ and $Au^{III}Cl_3$ salts, as well as the ligated cationic $[L\text{-}Au^{I}]^+$ and $[L\text{-}Au^{III}\text{-}Cl_2]^+$ catalysts. The benefit of ligated gold over the simple salts is improved stability and ability to fine-tune the electronic properties of the gold-centre, like electrophilicity.[32] Typical ligands for gold are phosphine and phosphate based, or N-heterocyclic carbenes (NHC), and the R-groups of the ligand are used to create steric bulkiness to stabilise the catalyst, see Scheme 2.1.

Gold(I) prefers linear bicoordinate complexes,[33] while gold(III) complexes are tetracoordinate and square planar.[34] The ligated gold complexes do not have low-lying vacant orbitals that could activate π-systems but the pre-catalytic form is activated by replacing one of the ligands from $L\text{-}Au^{I/III}\text{-}X_n$ (X = Cl, Br, I; n = 1, 3) with loosely-coordinating counterion, see **1** in Scheme 2.1. The anion metathesis is often carried out with silver salts and the counterions are usually conjugate bases of strong acids, *e.g.*, *p*-TsOH, $HNTf_2$, and $HF{\cdot}BF_3$.

Although AgCl precipitates from the solution, the silver present can have catalytic effects that either accelerate or inhibit the gold-catalysed reaction.[35] Other ion exchange methods include Au-Cl bond activation with NaX salts,[36] as well as the demethylation of L-Au^{I}-CH_3 with a strong Brønsted acid.[37]

Alternative ways of generating active gold-catalysts, which do not require ion exchange, include using side-arms in ligands that create the vacant site. Originally, Hashmi *et al.* demonstrated that a pyridine-$Au^{III}Cl_3$ complex and its derivatives increase the stability and recyclability of the gold catalyst over an $Au^{III}Cl_3$ salt,[38] while Pápai and Erdélyi showed that the vacant site is created by substitution of the pyridine moiety.[39] Limbach and coworkers[40] demonstrated that a pyridine side-arm tethered NHC ligand with Au(I) could form a stable and highly catalytically active dimer. Later, Helaja and coworkers[41] demonstrated that the same ligand design can be used to create an active site in a gold(III)-catalyst by replacing one chloride with a hemilabile Au-N coordination. Importantly, this activation method was most efficient in hydrogen bond donor solvents or in the presence of hydrogen bond donor additives, such as chloroform and 1,1,1-trifluoroethanol. Additionally, Michelet and coworkers[42,43] showed that the Au-Cl bond is efficiently activated with the same pyridine-tethered ligand with a supplementary sulfonic acid side-arm.

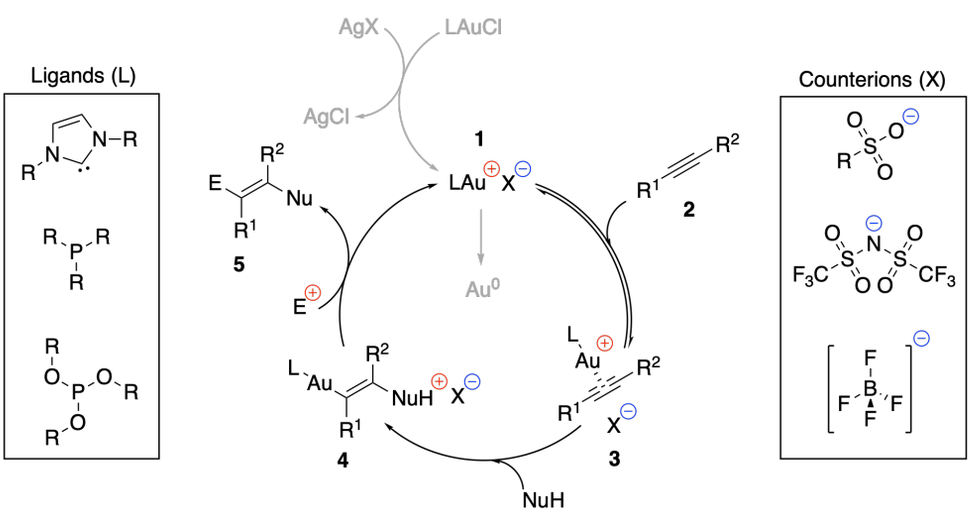

Scheme 2.1. Simplified catalytic cycle with homogeneous gold-catalysts.

The activated gold-catalyst **1** coordinates a C-C -system, *e.g.*, alkyne **2**, and forms a η^2-complex **3**, which then undergoes a Markovnikov-type nucleophilic trans-addition to the alkyne and forms a vinyl gold-complex **4**. However, reports of anti-Markovnikov hydroamination[44] and the mechanistic reasoning[45] have recently been published.

In the last step, a suitable electrophile, for example, a proton, releases

the gold catalyst back to the catalytic cycle and yields the product **5**, see Scheme 2.1. Although protodeauration is considered to be the rate-determining step in many gold-catalysed reactions, it is not always clear what species mediates the proton transfer. Usually, it is considered that the counterion is the proton transfer agent;[46,47] and often, a counterion with intermediate acidity and gold-affinity are utilised in reactions where protodeauration limits the rate of the reaction.[48] Alternatively, depending on the reaction, both substrate and product can mediate the protodeauration[49] and, furthermore, water can transfer the proton.[50–52]

The choice of ligand and counterion combination has a significant effect on the reaction rate[53,54] and should be chosen based on their combined effect. For example, electron-donating ligands increase the rate of protodeauration, whereas electron withdrawing ligands can assist in the nucleophilic addition.[55] At the same time, counterions with good hydrogen bond accepting ability can increase the rate of protodeauration, whereas counterions with high affinity for gold can act as inhibitors.[48]

2.2 Redox potentials and acid-base chemistry

Acidity and redox potentials are often discussed in the context of aqueous environment. However, organic chemistry is typically carried out in organic solvents where the measurement of $pK_{a(H)}$ and redox potentials can be challenging.[56,57] Simultaneously, acidities in non-aqueous and aqueous environments are not necessarily even qualitatively comparable.[58] Moreover, redox behaviour of organic molecules can be significantly different between water and organic solvents.[59,60] The difference in behaviour originates from the solvent-solute interactions: water can efficiently stabilise ionic species, whereas aprotic and non-polar organic solvents, such as dichloromethane (DCM), cannot. Proton and electron transfers often play a crucial role in several reactions, including those studied in the present work, and thus accurate prediction of these properties becomes important. One approach to evaluate acidity and redox potentials is to use quantum chemical methods – introduced in Chapter 3. The oxidation or reduction potential of a molecule is calculated from the reaction free energy in equation 2.1:

$$E^{\circ} = -\frac{\Delta G}{nF} - E^{\circ}_{ref} \tag{2.1}$$

Where ΔG is the free energy change between oxidised and reduced state, n is the number of transferred electrons, F is the Faraday's constant, and E°_{ref} is the potential of a reference electrode. Since the (computational) ΔG refers to an absolute redox potential, one should subtract the absolute potential of the reference electrode in order to compare computational values with experimental values. IUPAC recommends to use the ferrocenium/ferrocene (FcH^+/FcH) couple as the reference electrode in non-aqueous solvents,[61] but the standard calomel electrode (SCE) is also often utilised to report redox potentials.

The redox potential of chemically irreversible electron transfer can be calculated from the reaction free energy for the overall process, but the competing reaction pathways have to be known.[62,63] For example, under inert conditions in dry acetonitrile, nitrobenzene undergoes reversible one-electron reduction, while the process becomes irreversible in the presence of an acid.[64]

The acidity of neutral and cationic acids is calculated from the dissociation free energy of the acid in equation 2.2:

$$pK_{a(H)} = \frac{\Delta G}{RT\ln(10)} \tag{2.2}$$

Where ΔG is the acid dissociation reaction free energy, R is the gas constant, and T the temperature in Kelvin. Experimental acidity and basicity values

have been measured in different non-aqueous solvents,[65] and, for example, Leito's research group administers a database for acidities[66] and basicities[67] in different organic solvents.

Importantly, acidities and basicities can often be correlated with different organic solvents, given that the solvation effects are similar.[65] Impurities such as water, even in small quantities, can significantly change the proton activity.[68] In less polar solvents, such as 1,2-dichloroethane (DCE), ions exist predominantly as pairs or larger aggregates[69] so acidities in low-polarity organic solvents often correspond to the acidity of the forming ion pair[70,71] – either as a contact ion pair or solvent separated ion pair. The ion pairs are held together by Coulombic and weak interactions, and the nature of the interaction depends on the ions' steric bulkiness and ability to delocalise charge. The direct implication of ion pairing is that, for ions with small and localised charges, the ion pairing increases detected ion stability, *i.e.*, basicity or acidity is increased compared to the free ion.[72] Similar enhancement of ion stability can be detected in more polar solvents, for example, in acetonitrile where the conjugate bases of weaker acids form hydrogen bonds with the neutral acid and stabilise the localised charge.[65]

2.3 Photoredox chemistry

Visible-light photoredox catalysis is a class of catalysis where a photosensitiser is excited with light and, as a result, the excited state catalyst transfers the energy to a substrate either *via* electron transfer (ET) or energy transfer. The ability of visible-light photocatalysis to complement the conventional organic synthetic methods, *i.e.*, closed-shell two-electron movements, was recognised at the end of 2000s by three separate groups[73–75] and has since undergone remarkable growth. Commonly used photocatalysts include TM complexes[76] and organic dyes.[77] The most widely used TM photocatalyst, $[Ru(bpy)_3]^{2+}$, which has been extensively studied since the 1950s,[78] was used in the Publication II as the photocatalyst in photoreduction of nitro heteroarenes. The general process of electron and energy transfer with a photocatalyst is presented with $[Ru(bpy)_3]^{2+}$, abbreviated as $[Ru^{2+}]$.

Irradiation of $[Ru^{2+}]$ at 452 nm[79] excites one electron from the metal-centred t_{2g}-orbital (ground state) to the ligand's π^*-orbital (excited singlet state)[80] in a process known as metal to ligand charge transfer (MLCT), see Scheme 2.2. The singlet MLCT state then undergoes intersystem crossing (ISC) to the lowest energy triplet MLCT state ($^3[^*Ru^{2+}]$),[81] which has a lifetime of around 1100 ns.[82]

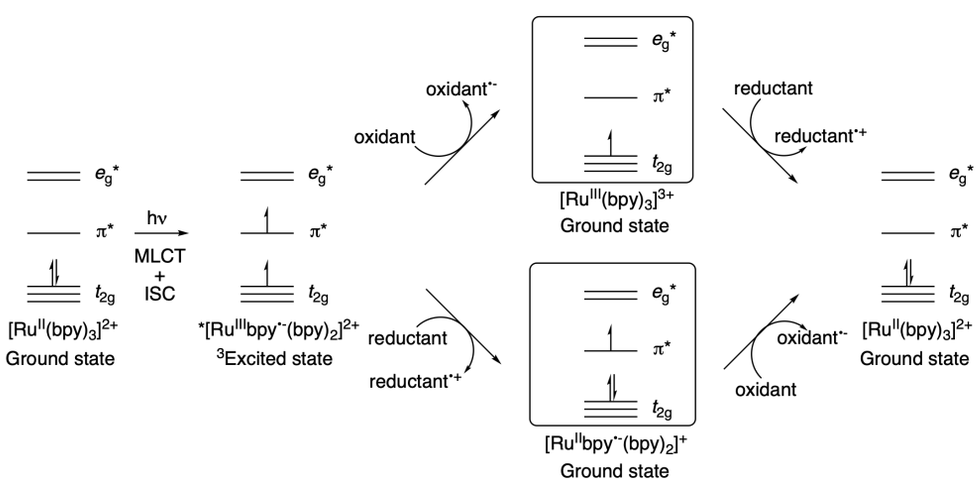

Scheme 2.2. Oxidative and reductive quenching cycles of $^3[^*Ru(bpy)_3]^{2+}$.

The excited $^3[^*Ru^{2+}]$ can then be either oxidatively or reductively quenched with an electron acceptor or an electron donor, respectively. The reduction potential of $^3[^*Ru^{2+}]$ is -0.81 V while the oxidation potential is 0.77 V.[83] The formed $[Ru^{3+}]$ or $[Ru^{+}]$ species is then reduced (1.29 V) or oxidised (-1.33 V),[83] respectively, to yield the ground state $[Ru(bpy)_3]^{2+}$. When considering the feasibility of redox reactions, König[84] has introduced a rule-of-thumb that

ΔG must be thermoneutral or exergonic for ET processes involving an excited state photocatalyst, because of the short lifetime of the excited state. For example, the 1100 ns lifetime of $^3[^*Ru^{2+}]$ is equivalent to $k = 9.1{\cdot}10^5$ s^{-1} or $\Delta G^{\ddagger} = 9.3$ kcal/mol for a first-order decay at room temperature. For the ground-state photocatalyst, the ΔG for ET can be positive by up to 0.5 V.[84]

To evaluate the activation free energy barrier of an electron transfer between the excited state photocatalyst and the substrate, the Marcus theory[85–87] can be utilised. The Marcus theory evaluates the rate from the free energy difference between the substrate and product states and the solvational and vibrational reorganisations involved in the process. Generally, it can be concluded that, in the normal region, the rate is higher for more exergonic electron transfer processes. Thus, an exergonic electron transfer reaction can have a rate that competes with the rate of the decay of the excited state of the photocatalyst. The reader is advised to refer to review articles of the Marcus theory for more theoretical background.[87,88]

The $^3[^*Ru^{2+}]$ can also be quenched *via* an energy transfer processes in addition to ET. In collisional energy transfer, also known as the Dexter energy transfer,[89] the electrons are formally exchanged between the $^3[^*Ru^{2+}]$ and S (for substrate), see Scheme 2.3, but the total spin of the system is preserved. This means that either the triplet state of the ^{3}PC or singlet state of ^{1}PC is transferred to S and ^{3}S or ^{1}S is produced, respectively. The T_1 energy of $^3[^*Ru^{2+}]$ (2.02 V)[82] must be greater than or equal to the triplet state energy of the acceptor, S, in addition to sufficient overlap of the donor and acceptor wavefunctions.[89]

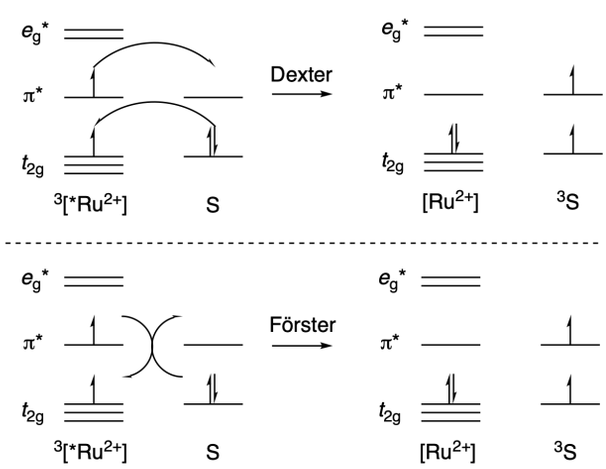

Scheme 2.3. Energy transfer schemes from excited $^3[^*Ru^{III}bpy^{\bullet-}(bpy)_2]^{2+}$ to acceptor S.

In the Förster mechanism, see Scheme 2.3, the energy transfer does not require collision between $^3[^*Ru^{2+}]$ and S, but can occur at very large inter-

molecular distances.[89] More importantly, some amount of spectral overlap must exist between the emission spectrum of $^3[^*Ru^{2+}]$ and the absorbance spectrum of S. The Förster mechanism is more often associated with singlet state energy transfers – change excited electron to spin-down in Scheme 2.3 – but the process is otherwise analogous to the triplet process in Scheme 2.3. Both Dexter and Förster-type energy transfer processes are non-radiative. The thermochemical properties of $[Ru(bpy)_3]^{2+}$ are summarized in Scheme 2.4.

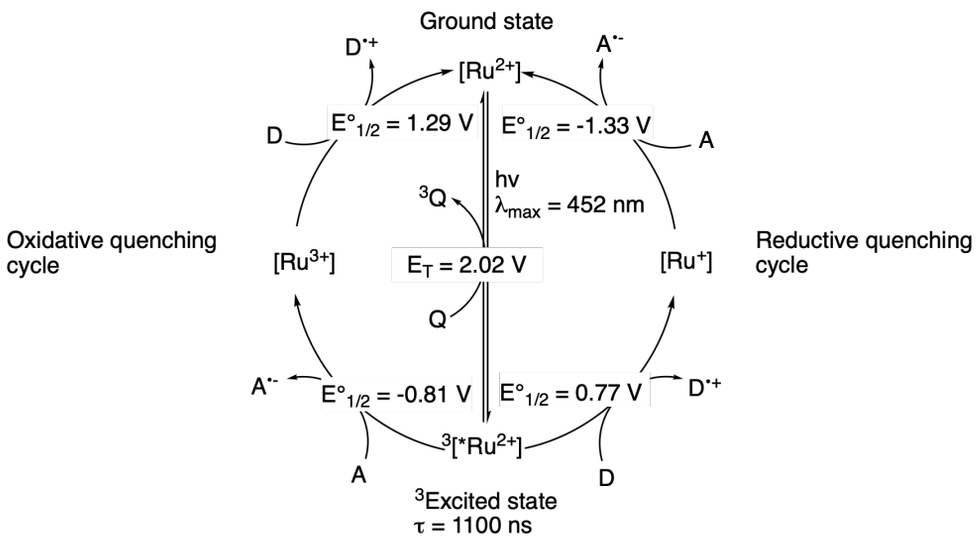

Scheme 2.4. Thermochemical properties for $[Ru(bpy)_3]^{2+}$ and its excited state.[90] A stands for electron acceptor, D for electron donor, and Q for quencher.

Although the energy transfer process is less employed in synthesis, it can be utilised to excite and activate more potent reductants and oxidants. For example, König and coworkers demonstrated[91] that $^3[^*Ru^{2+}]$ can excite anthracene *via* triplet-triplet energy transfer (TTET) to triplet anthracene species, which is quenched by an electron donor. The anthracenyl radical anion is subsequently a more powerful reductant (-1.95 V) than $[Ru^+]$ (-1.33 V). Determination of the operative mechanism is not always trivial,[92,93] but techniques such as time-resolved emission spectroscopy can help to find the plausible mechanisms.[90,94]

To determine what chemical species quenches the excited state photocatalyst, Stern-Volmer measurements are routinely employed.[95] In principle, the Stern-Volmer measurements are carried out by exciting the photocatalyst with the correct wavelength and increasing the concentration of the quencher between experiments while keeping the concentration of the photocatalyst constant. The emission intensity of the excited state photocatalyst is then measured and the relationship between the emission intensity and [Q] is then expressed as:

$$\frac{I}{I_0} = 1 + k_q \tau_0 [Q] \tag{2.3}$$

Where I and I_0 are the emission intensities with and without the quencher, respectively; k_q is the quenching rate constant; τ_0 is the excited-state lifetime of the photocatalyst; and [Q] is the concentration of the quencher. The plot I/I_0 versus [Q] can be used to find the quencher reagent in the reaction or a combination of reagents and offer mechanistic information on the quenching event.[96] For example, Qiu and Knowles demonstrated that negative curvature of the Stern-Volmer plot indicates association of the electron and proton acceptor with the proton donor, or *vice versa*, prior to the quenching of the excited state photocatalyst.[96]

2.4 Proton-coupled electron transfers

Electron transfer (in photoredox) reactions are often coupled with proton transfer (PT), which comprise an important class of bond reorganisations. The ET-PT event can either be concerted proton-electron transfer (CPET), where proton and electron move in concerted manner and no intermediate is formed; or it can be a sequential proton-electron transfer (SPET) where a distinct intermediate forms between the PT and ET, see Scheme 2.5. In Publication II, we investigated the nature of ET-PT events in photoreduction of nitro N-heterocycles and explored the mechanism from a thermochemical perspective: whether the electron, proton, or proton-coupled electron, transfer step is energetically feasible or favoured. While the thermochemistry does not directly indicate the kinetic feasibility of the step, it can be used to exclude intermediates with high reaction free energies. The mechanistical perspectives for PT-ET processes is given below.

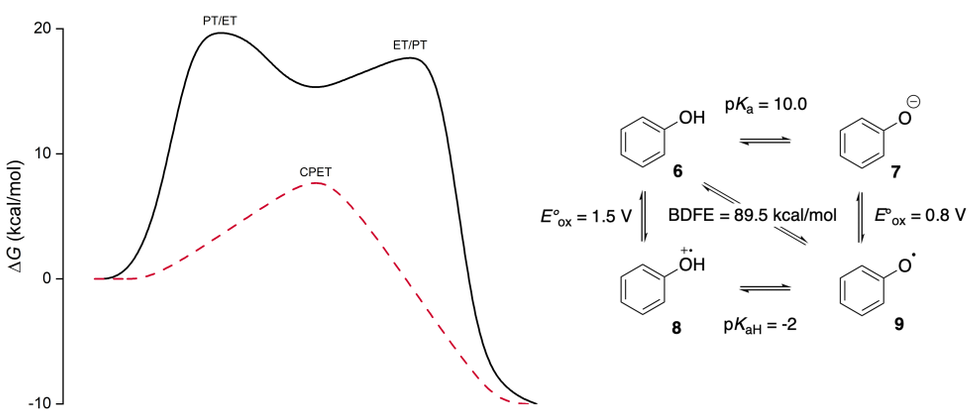

Scheme 2.5. On the left: schematic energy profiles for an imaginary SPET (solid black line) and CPET (broken red line) processes. On the right: square diagram of e^-/H^+ thermochemistry for phenol **6** and phenoxyl radical **9**. The $pK_{a(H)}$, E°, and BDFE values are measured in water.[59]

Although the product of both stepwise and concerted processes is the same in Scheme 2.5, the energy profile changes drastically. For example, deprotonation of phenol **6** with a base ($pK_{aH} \geq 10$) makes the subsequent oxidation of phenolate **7** feasible. On the other hand, one-electron oxidation of **6** with a strong oxidant ($E^\circ_{ox} \geq 1.5$ V) in turn generates a high-energy species, the phenoxyl radical cation **8** that is easily deprotonated.

CPET is often thermodynamically favoured over SPET because ΔG for the CPET process is always lower than for the first step of SPET, see Scheme 2.5.[97] The square-diagram in Scheme 2.5 can be used to calculate the $\Delta G(298\ \mathrm{K})$ for

homolytic bond dissociation free energy (BDFE) of phenol's O-H bond from equation 2.4:[59]

$$BDFE_{solv}(X-H) = 1.37\mathrm{p}K_{a(H)} + 23.06E^{\circ} + \Delta G_{solv}(H^{\bullet}) \tag{2.4}$$

where BDFE is in kcal/mol, $\mathrm{p}K_{a(H)}$ is the acidity of the acid or base, E° is the redox potential of oxidant or reductant in V, and $\Delta G_{solv}(\mathrm{H}^{\bullet})$ is the free energy of solvation of a hydrogen atom in the given solvent in kcal/mol.[59] The values for $\mathrm{p}K_{a(H)}$ and E° in equation 2.4 must be for the consecutive steps, *e.g.*, $\mathrm{p}K_a = 10$ and $E^{\circ} = 0.8$ V in Scheme 2.5. BDFE-values can be used to compare the thermochemistry between hydrogen atom acceptor and donor analogously to comparing $\mathrm{p}K_{a(H)}$ and E°-values.

The CPET reactions can be divided into sub-categories depending on whether the $\mathrm{e}^-/\mathrm{H}^+$ transfer takes place between two molecules – hydrogen atom donor and acceptor – or between a triad of donors and acceptors. In hydrogen atom transfer (HAT) reactions that take place between two molecules, the proton and electron are transferred roughly via same path. A classic example of such a process is the self-exchange reaction of a hydrogen atom between toluene and a benzyl radical, where the proton transfer coordinate and the SOMO p_{π} orbital are aligned along the same vector.[98]

In the proton-coupled electron transfer (PCET) mechanism between two molecules, which is similar and often difficult to distinguish from HAT,[97,99] the electron moves via an orthogonal orbital compared to the vector of proton transfer. The self-exchange reaction between phenol and the phenoxyl radical transfers the electron between the oxygen π orbitals[98] or between the π-stacked phenyl rings,[100] while the proton is transferred between the σ lone pairs.

Hydrogen bonding or the lack of it between the $\mathrm{e}^-/\mathrm{H}^+$ donor and acceptor determines whether the mechanism is PCET or HAT, respectively, because without preformation of the hydrogen bond complex the PCET mechanism is not possible. The preformation of the hydrogen bond complex, however, does not exclude the HAT mechanism, but π donating groups favour PCET over the HAT mechanism.[98] Although the above distinctions are not quantitatively rigorous,[101] they have been shown to be qualitatively consistent.[102,103] The reader is advised to refer to good review articles of the physical chemistry aspects of PT-ET reactions.[101,104]

PCET reactions are not restricted to take place between one acceptor and one donor, but electron and proton can be accepted (donated) from one molecule to two separate molecules, see Scheme 2.6, and the effective BDFE for the ac-

ceptors (donors) is estimated with equation 2.4. Analogous to single site PCET reactions, the multisite proton-coupled electron transfer (MS-PCET) is thermodynamically favoured over the SPET reaction, for example, in reduction of ketones[96] (**11** in Scheme 2.6), and oxidation of phenols[105] (**6** in Scheme 2.6). Importantly, the hydrogen bond complex forms between proton acceptor and proton donor prior to electron transfer. Intriguingly, a recent report from Knowles demonstrated that a non-covalent oxidant-base hydrogen bond complex of an excited-state *Ir(III)-photocatalyst and monobasic phosphate base facilitated analogous C-H bond MS-PCET with non-activated alkanes.[106]

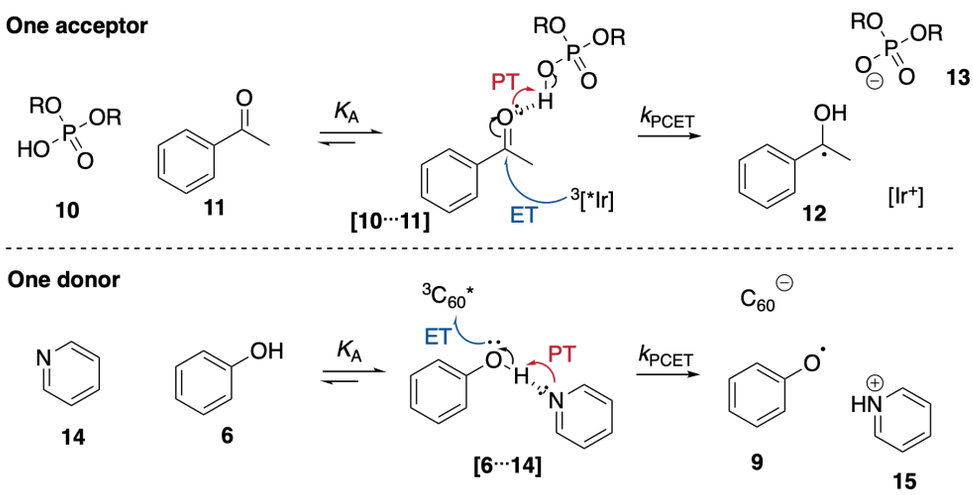

Scheme 2.6. Two different MS-PCET reactions. Above: the proton and electron are transferred to same molecule from two different donors.[96] Below: the proton and electron are accepted by separate species from one donor.[105]

The significance of CPET reactions has been recognised in biological systems, for example, Photosystem II[107] and Cytochrome Oxidase,[108] and importantly CPET reactions have been acknowledged as a mean to generate radicals with homolytic bond activation in synthetic chemistry.[109,110] The direct HAT reactions can often suffer from the limitation that the ΔG of the HAT reaction must be exergonic or thermoneutral.[111] Typically this is achieved with high-energy heteroatom-centred radicals that pose a limitation for the method. On the other hand, use of site-separated proton acceptors (donors) and electron acceptors (donors) can facilitate homolytic bond breakings with effective BDFEs of 110 kcal/mol,[111] and reports of endergonic MS-PCET reactions exist.[112,113]

2.5 Liquid-phase oxidative dehydrogenative C-C couplings

Oxidative dehydrogenative (ODH) C-C couplings were discovered in 1868[114] and have remained relevant for over 150 years. ODH C-C couplings are readily carried out without pre-functionalisation or guiding functional groups unlike many TM-catalysed C-C bond formations[115] and the forefront of the field is in aryl cross-coupling reactions and nanographene synthesis.[116] Conceptually, the ODH C-C coupling of aryls can be divided into two mechanistically different classes: i) the one-electron oxidation initiated pathway that forms a radical cation as the reactive intermediate; and ii) protonation and formation of arenium cation as the reactive intermediate, see Scheme 2.7. The operative mechanism, however, often remains elusive in reactions, but general guidelines have been drawn for both mechanisms.[115]

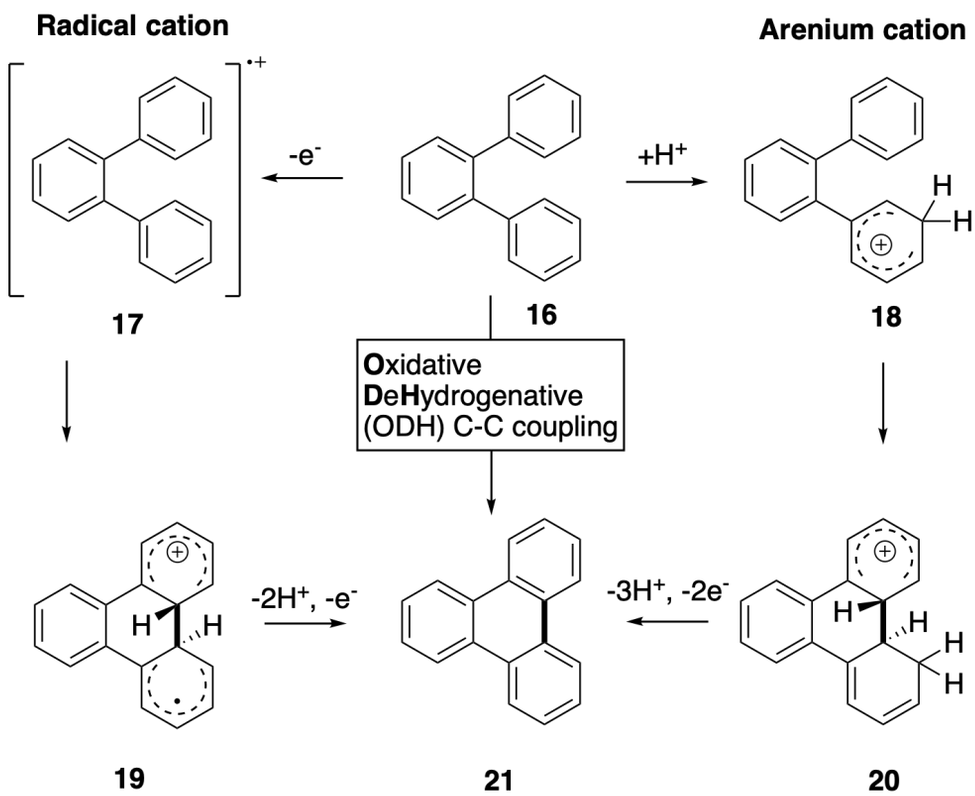

Scheme 2.7. Schematic presentation of the radical cation (left) and arenium cation (right) ODH C-C coupling mechanisms.

The radical cation C-C coupling – or oxidative aromatic coupling – is distinctively carried out with electron rich substrates, such as phenols or alkyl aryl ethers and oxidants or oxidising Lewis acids, for example, $FeCl_3$[117] and $MoCl_5$.[118] Single-electron oxidation of **16** initiates the reaction and forms **17**,

a radical cation where the spin-density localises on the most electron rich position of the neutral form. The radical cation then reacts with a nucleophile, which in this case is intramolecular, and yields a distonic radical cation **19**. Subsequent $e^-/2H^+$ oxidation delivers the final triphenylene product **21**.

The arenium cation mechanism – Scholl reaction – is carried out with less electron rich substrates than the radical cation counterpart and with non-oxidising Brønsted or Lewis acids, for example $AlCl_3$,[117] and additional oxidant.[119] In the first step – with Brønsted acid – protonation of the aryl ring (**18**) activates the substrate for nucleophilic addition (**20**). The following deprotonations and oxidation then generates the final triphenylene product **21**.

Yet, ODH aryl C-C coupling reactions often deliver surprising products that are not predicted prior to carrying out the reaction, but consideration of alternative computed mechanistic pathways usually explains the product formation.[120,121] Both radical cation and arenium cation mechanisms have supporting computational[24] and experimental[25,122] evidence, but the ability of the utilized Lewis acid, *e.g.*, $FeCl_3$, to act as an oxidant[115] brings ambiguity over the operative mechanism.

In addition to TM salts, quinones mediate the ODH aryl C-C coupling and the DDQ/H^+ system is often used.[25,123–125] Other reagent combinations with the quinones include hydrogen bond donors[126–128] and Lewis acids[129,130] that also facilitate the electron transfer. The Brønsted acid additive enhances the oxidative power of quinone[128] either *via* an MS-PCET or SPET mechanism, see section 2.3, but can also protonate the substrate.[119,122]

2.6 Molecular quinones as models for active sites in carbon materials

The catalytically active sites in carbon materials for oxidation reactions are typically considered to be the quinoidic groups impeded on the carbon surface based on functional group blocking,[131,132] computations,[133–136] correlating the activity with the amount of C=O groups,[132,137,138] and replication of activity with molecular quinones.[139–141] Various reports have demonstrated how adjacent hydrogen bond donor groups to carbonyls increases the reduction potential of molecular quinones[60,127] and, likewise, the presence of carboxylic and hydroxylic groups in carbon materials can be verified with X-ray photoelectron spectroscopy.[142] Importantly, the intramolecular hydrogen bonding between carbonyls and hydrogen bond donors can block the intermolecular hydrogen bonding and decrease the effect of acid additives.[127]

Nevertheless, the quinoidic group topologies, as well as the relative locations of other functional groups in the carbon materials, remain elusive. Instead of designing representative model quinoidic fragments with different functional group patterns for different carbon materials, *e.g.*, oxidized carbon nanotubes (oCNT), graphene oxide, or oxidized active carbon (oAC), we used molecular quinones to model the reactivity. In Publication III, we experimentally tested phenanthrenequinone (PQ) and anthraquinone (AQ), see Scheme 2.8, in intermolecular ODH aryl-aryl C-C coupling. Both provided homocoupled product.

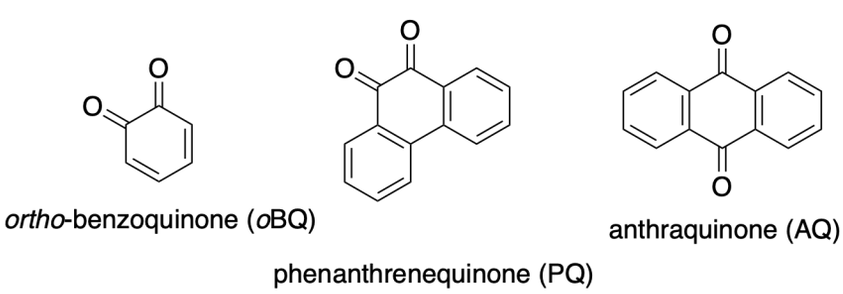

Scheme 2.8. Examples of molecular quinones used in the current work.

3. Methods

3.1 General

According to transition state theory (TST),[143] the rate of a chemical reaction can be calculated from the energy or free energy difference between minimum energy structures and transition states connecting them, for example, A $\rightarrow$ $[TS]^{\ddagger}$ $\rightarrow$ B. The reaction Gibbs free energy, which comprises enthalpic and entropic contributions ($G = H - TS$), is determined as the free energy difference, ΔG, between states A and B. The Gibbs activation free energy, $\Delta G^{\ddagger}$, is the free energy difference between A (B) and $[TS]^{\ddagger}$. The Gibbs activation free energy can be connected to experimental reaction rates obtained, *e.g.*, from reaction kinetic measurements, using the Eyring equation:[144]

$$k = \frac{k_B T}{h} e^{-\frac{\Delta G^{\ddagger}}{RT}} \tag{3.1}$$

where k is the reaction rate constant, k_B is the Boltzmann constant, T is temperature in K, h is the Planck constant, R is the gas constant, and $\Delta G^{\ddagger}$ is the Gibbs activation free energy. Computational methods, in particular quantum chemical methods, are typically employed to calculate experimental observables such as reaction rates and selectivity. Therefore, a short introduction to these methods is given below.

3.2 Computational methods

3.2.1 Background for wave function and density functional methods

The common computational quantum chemistry methods are based on wave function theory and density functional theory. The former method aims to solve the time-independent Schrödinger equation 3.2 to obtain the wave function of the system:

$$\boldsymbol{H}\Psi = E\Psi \tag{3.2}$$

where $\boldsymbol{H}$ is the Hamiltonian operator that describes the kinetic and potential energy of the system; Ψ is the wave function of the system depending on the position of the nuclei and electrons; and E is the total energy of the system with wave function Ψ. However, the wave function can only be solved exactly for one electron systems, such as the hydrogen atom. Consequently, various approximations have to be introduced.

An integral part of solving the Schrödinger equation is the Born-Oppenheimer approximation, where coupling of nuclear and electronic motions is neglected since nuclei are much heavier than electrons,[145,146] *i.e.*, the nuclear wave function and the electronic wave function can be treated separately. The electronic part can then be solved with nuclear positions as parameters on a potential energy surface.

Another crucial approximation is to consider the motion of one electron as independent of the motion of other electrons in the system. For example, in the Hartree-Fock (HF) method[147–149] a single Slater determinant is used to construct the wave function from one-electron orbitals meaning that the Pauli exclusion principle is satisfied. However, the electron-electron repulsion of opposite spins is neglected. To account for the electron-electron repulsion of opposite spins, all electrons of the system are treated as a mean-potential field arising from their average positions. Since the solution for both one-electron orbitals and mean-potential field depend on each other, they are solved iteratively until the functions no longer change and result in a self-consistent field solution. Since the effective field describes the positions of all electrons in the system, each electron therefore unphysically interacts with itself. The self-interaction error is, however, cancelled out by the electron exchange energy in the Hartree-Fock-Roothan equations.[145]

Although the HF method is the best solution for a single-determinant wave function and able to account for 99% of the total energy, the missing 1% is often

important to account for chemical accuracy. The HF method does not consider weak interactions that are important for describing, *e.g.*, dispersive forces and π-π stacking effects. The missing energy results from the omitted correlation of the movement of electrons that the mean-potential field fails to describe. Post-HF methods have been developed to incorporate the missing electron correlation and to systematically improve the HF result. Some of the most popular methods include configuration interaction (CI), second-order Møller-Plesset perturbation theory (MP2), and the coupled-cluster (CC) methods, especially the "gold standard" CCSD(T). For a more in-depth theory of these post-HF methods, the reader should refer to comprehensive computational chemistry books.[145,150]

Another widely used approach is based on density functional theory (DFT) and has become the *de facto* work horse in computational chemistry for organic chemistry and TM catalysis. Hohenberg and Kohn showed[151] that, according to the variational principle, the ground-state electron density determines the electronic energy of the system. Every molecule has a unique electron density that is an observable dependent of three variables: x, y, and z, positions in space,[150] instead of the $3n$ spatial coordinates in wave function theory, where n is the number of electrons in the system. Although the result is very appealing, the major problem is that the exact functional connecting the electron density to the energy of the system is not known.

Kohn and Sham's theory formed the basis for contemporary KS-DFT methods with a general DFT energy expression, where a set of self-consistent equations are solved to find a set of spin orbitals that minimize the energy. The general KS-DFT energy functional is given by:[152]

$$E[\rho(\mathbf{r})] = T_e[\rho(\mathbf{r})] + V_{ne}[\rho(\mathbf{r})] + V_{ee}[\rho(\mathbf{r})] + E_{xc}[\rho(\mathbf{r})] \tag{3.3}$$

T_e is the kinetic energy for a system of non-interacting electrons with the density of the true interacting electrons; V_{ne} is the nuclear-electron attraction, which can be solved exactly; and V_{ee} is the Coulombic electron-electron repulsion of the electron density with itself. The procedure for solving the KS equations is also a self-consistent procedure: solve for the orbitals iteratively to minimize the energy. In the HF method, the electrons interact with an effective field describing the average positions of all the electrons in the system; while in DFT, the potential is constructed from the electron density of non-interacting electrons.[150]

The last term, the exchange-correlation functional E_{xc}, is the term that accounts for all other aspects of the true system and tries to redeem the ap-

proximations made to the kinetic energy and electron correlation. However, the exact form of the exchange-correlation functional is unknown, so practical implementations of DFT only include electron correlation approximately. Consequently, density functionals focus on approximating the E_{xc} with different approaches. The different functional classes are introduced below; more thorough theoretical descriptions of DFT methods can be found in comprehensive introductory computational chemistry books.[145,153,154]

3.2.2 Different density functionals

The local density approximation (LDA) approximates the electron density as an uniform electron gas, and assumes that the exchange energy can be determined from the density alone.[150] The LDA has been extensively applied in material sciences, where the uniform electron gas approximation is sufficient for (infinite) material surfaces. For molecular systems, however, LDA gives a poor performance as it overestimates bond dissociation barriers by up to 30 kcal/mol.[155]

The LDA can be improved by including derivatives of the electron density, for example, the gradient of the electron density in order to account for the non-homogeneity of the true electron density, in addition to enforcing the rules for Fermi and Coulomb holes.[153] The functionals in this class are called generalised gradient approximation (GGA) functionals. Quite intuitively, to improve GGA, one can allow the exchange and correlation functionals to depend on higher-order derivatives of the electron density, such as the Laplacian of the density and orbital kinetic energy, and this class of functionals is called *meta*-GGA (mGGA).[145]

The GGA and mGGA improve significantly over the LDA[155] yielding a systematic performance over a wide range of systems. An example of a GGA functional is the fast and robust BP86[156,157] functional;[158] and an example of a mGGA functional is the TPSS,[159] which gives a good performance across the periodic table[1,160] with TM complexes,[161–164] and importantly with gold complexes,[165,166] which is why the functional was used in this work.

On the next rung are the hybrid functionals, where a fraction of exact exchange from the HF theory is mixed with the (m)GGA exchange-correlation functional. The addition of exact exchange reduces the self-interaction error introduced from the calculation of Coulombic electron-electron repulsion that in DFT cannot be cancelled out. Depending on how a hybrid functional is built, the fractional amount of HF exchange can vary; but a greater amount of exact HF exchange can yield better results for geometries[167] and energies.[168,169] However, the functional cannot be systematically improved by

increasing the amount of HF exchange as it can lead to overestimated barriers, over-stabilisation of high-spin states, and typically a bad description of transition states.[145]

The most popular density functional, B3LYP (20% exact exchange),[170–172] belongs to this category, and other examples include PBE0 (25% exact exchange)[173] and PW6B95 (28% exact exchange).[174] Comparison studies show that the accuracy of these functionals to predict thermochemistry, kinetics, and noncovalent interactions of organic molecules, is improved over LDA and (m)GGA functionals.[160] Additionally, it has been demonstrated that PBE0 and B3LYP perform well for geometries.[163,166,175] For energies, PBE0 and B3LYP perform similarly,[1] and Grimme's extensive general chemistry benchmarks[1,160] recommend the dispersion corrected PW6B95-D3(BJ) as the most robust and very accurate general purpose global hybrid. The PBE0 and PW6B95 functionals were used in this work.

Further advances include the class of double-hybrid functionals, where a fraction of MP2 correlation is added to a hybrid functional. An example of such a functional is the B2-PLYP developed by Grimme.[176] Additional approaches include the random-phase approximation[7] that captures the non-pairwise additive nature of long-range interactions accurately and includes dispersion interactions in a seamless manner without empirical parameters.[155]

3.2.3 Thermochemistry

The quantum chemical methods introduced above are used to calculate energies at 0 K. In order to obtain the Gibbs free energies that are commonly used in calculations on organic molecules, one must compute vibrational frequencies from the Hessian matrix that can be estimated based on a rigid-rotor harmonic oscillator (RRHO) approximation. The thermal corrections and vibrational frequencies obtained in this way are often overestimated, since the real vibrational frequencies are anharmonic,[145] whereas the RRHO approximation treats them as harmonic. The overestimation, however, is often systematic and scaling factors have been proposed for different functional/basis-set combinations.[177] The frequency calculations are, however, prone to errors and therefore can introduce significant errors when calculating vibrational entropy contributions.[178] Different approaches to counter these errors have been suggested,[179–181] and in this thesis we used the approach suggested by Grimme.[182] In this approach, the contribution of the vibrational modes below 100 cm^{-1} is treated as free-rotor entropy, since the quasi-RRHO approximation is considered more reliable for systems with many vibrational modes below 100 cm^{-1}.[182]

Conformational sampling is another important factor that can be used to

further improve the results for flexible molecules, because if wrong conformer is chosen, the energetics for a process can be qualitatively wrong. Since the amount of conformers grows as $3n$, where n is the amount of freely rotatable bonds, even reasonably small molecules have a large amount of conformers, which need to be sampled. Several programs and algorithms have been used in the literature to map the conformer space, for example, iterative dihedral scan[183] and RDKit,[184,185] but here we use the CREST program package,[11] which aims to find the low-energy conformers using meta-dynamics incorporated with GFN-xTB.[10]

3.2.4 Specific problems with DFT

A significant short-coming of DFT is the self-interaction error, which means that the electron unphysically interacts with itself.[186,187] The self-interaction error originates from the calculation of the Coulomb electron-electron repulsion, where the electron interacts with a potential that is constructed from the whole electron density. In HF theory, on the other hand, the two-electron integrals include electron exchange energy that completely cancels out the self-interaction error; but such cancellation is not possible in DFT because the exact exchange-correlation functional is not known. For this reason, DFT typically predicts the electron density to be delocalised and fails to predict structures where the charge and spin are localised[188] to dissociate atoms even at large intermolecular[168] and interatomic[169] distances. For example, pure DFT functionals fail to describe asymmetric transition states for symmetric butadiene radical cations, but an admixture of exact exchange will allow for the transition states to be optimised.[188] Additionally, the self-interaction error causes the electrons to be more loosely bound. This is evident, for example, in systematic underestimation of oxidation potentials;[124] but a hybrid functional can reduce the errors.

A practical problem with the current density functional approximations is that they cannot describe long-range electron correlation.[189] There are several *ad hoc* ways to introduce dispersion interactions,[190,191] for example, Head-Gordon's long-range corrected dispersion functionals.[192] In this work, we used the method introduced by Grimme and coworkers.[4,5] The dispersion energy is included without an extra computational cost and it has been demonstrated that the zero-damped (D3)[4] and Becke-Johnson (D3BJ)[5] dispersion corrections systematically improve the results for almost all density functionals.

3.3 Basis sets

3.3.1 Basis set families

Basis sets, which are constructed using either Slater-type orbitals (STOs) or Gaussian-type orbitals (GTOs) as basis functions, are used to approximate atomic orbitals that *via* linear combinations construct the molecular orbitals.[145,150] STOs mimic the exact solution of the Schrödinger equation for the hydrogen atom, but solving some of the integrals for STOs is not analytically possible and they have to be numerically evaluated. This can be avoided with GTOs so they are used more often. However, unlike the STOs, a single GTO does not describe the one-electron solution adequately. The problem can be overcome by combining a number of GTOs to describe a basis function: for example, STO-3G is constructed from three GTOs.

The construction of different basis sets has been reviewed and a detailed overview is presented in introductory computational chemistry books.[145,193,194] The following discussion will outline the conceptual differences between different basis sets and the aspects of choosing a sufficient basis set for a given problem within the context of the current work. In this thesis, we have used the Karlsruhe basis sets[195,196] exclusively so the discussion focuses on them. The Karlsruhe basis sets are available for all elements up to radon ($Z = 86$) and they include complementary auxiliary basis sets for the resolution-of-identity (RI) approximation[197] as well as for effective core potentials.

The most coarse basis set has one basis function per occupied atomic orbital: 1 s-type for H, 2 s-type and 3 p-type for C, and 3 s-type and 6 p-type for S. This is referred to as the minimal or single-zeta (SZ) basis set, where zeta (ζ) represents the basis functions. An example of the minimal basis set is the STO. The single-ζ basis set is, unfortunately, not suitable for studying the chemistry of molecules as the basis set is not flexible enough so more basis functions are used to describe the atomic orbitals. A straightforward solution is to double (D), triple (T), quadruple (Q) or quintuple (5) the amount of basis functions compared to single-ζ which results in DZ, TZ, QZ and 5Z basis sets, respectively. The amount of basis functions, on the other hand, increases the computational cost, so this is not a cost-efficient strategy to achieve better accuracy.

A more frequently utilised strategy is to divide the atomic orbitals into core and valence orbitals and introduce the additional basis functions only for the valence orbitals as they are important for the observed chemistry. The basis sets constructed in this way are called split-valence basis sets and, for example,

a split-valence DZ has twice as many basis functions for the valence orbitals as SZ, but the core is represented at the SZ level. Nevertheless, the basis functions added in this manner do not provide for mathematical flexibility: orbitals on hydrogen will remain spherical since only s-type orbitals are added and bent bonds are not described well.[150] Higher angular momentum functions, *e.g.*, additional p-type function for s orbitals and corresponding d-type functions for p orbitals, provide this flexibility and help to describe charge polarisation. These functions are called polarisation (P) functions. An example of a split-valence DZP basis set is the Ahlrichs def2-SVP basis set,[196] where the SVP stands for split-valence polarized.

When small anions, atoms with lone pairs, or electron affinities are studied it is recommended to use basis sets augmented with diffuse functions[150] as they allow the electron density to expand into a larger space. An example of Karlsruhe diffuse-augmented basis set is the def2-TZVPD.[198]

3.3.2 Specific problems with basis sets

Since using complete basis sets for molecular applications is not possible in practise, each molecular orbital is described with a finite number of basis functions. As a result, if the basis set size is too small, the electron density centred on one nucleus can be partly described by basis functions centred on other nuclei.[150] For example, when binding two molecules A and B, the respective basis sets of molecule A are used to describe i) A's electrons, ii) electrons involved in binding of A and B and iii) some of the electrons of molecule B. The same is true for the basis sets of molecule B. This can lead to overstabilisation in dimerization energies. The easiest way to circumvent basis set superposition error is by increasing the amount of basis functions until the interaction energy converges.

Typically, it is considered that qualitatively correct results are achieved using DZP level basis sets for DFT and HF methods while quantitatively correct results are achieved with TZP basis sets; but the convergence should always be checked. Generally, it is recommended to use the largest possible basis-sets for the studied system, as was done in this thesis. Furthermore, because Publications II–V involved systems with small anions, atoms with lone pairs and accurate prediction of redox properties for different systems, we used the diffuse-augmented basis set def2-TZVPD to report the final energies.

3.4 Solvation models

During the early days of computational chemistry, modelling of reaction mechanisms was performed in vacuum as solvation models were not generally available. Although geometries and relative energies in vacuum and in solvent environment are often different,[199,200] the gas-phase computations could effectively explain selectivity and reactivity. The success of computing geometries and energies in vacuum comes from cancellation of solvation effects if the errors introduced by the vacuum are similar in different reaction pathways. However, for ionic species, solvation effects can significantly influence even molecular structures.[178]

Today, solvation models are routinely used in computations and a popular variant of dielectric continuum solvation models (DCSMs) is the conductor-like screening model (COSMO).[3,201] Like other implicit DCSMs, COSMO approximates the solvent environment as a dielectric continuum and neglects all explicit interactions between the solute and the solvent. One can add explicit solvent molecules to model, for example, hydrogen bonding but the approach can give erroneous results if the system's degrees of freedom are not included properly.[178] Another shortcoming of the method is the inability to differentiate between two solvents with similar dielectric constant but different properties like cyclohexane ($\varepsilon = 2.02$) and benzene ($\varepsilon = 2.27$). Likewise, computation of the acidity of a molecule can be a difficult task due to strong charge localisation in anions and the need to account for the solvent-solute interactions in a physical way.

There are a few approaches to overcome this problem. One example is COSMO for realistic solvation (COSMO-RS) developed by Klamt *et al.*,[8,9,202] which is widely applied in chemical engineering. COSMO-RS combines COSMO with a statistical thermodynamics treatment of interacting charge surfaces from quantum chemical calculations. The COSMO-RS approach can take into account the solvent-solute interactions, such as van der Waals interactions and hydrogen bonding, thus improving over COSMO.[203] Other solvation models include the reimplementation of COSMO-RS, *i.e.,* COSMO segment activity coefficient (COSMO-SAC),[204] as well as the SMD[205] method of Truhlar.

The accuracy of COSMO-RS for predicting hydrogen bonding energies has been criticized as, for example, the hydrogen bonding to an anion can even be qualitatively wrong;[206] but it performs better when the species are neutral.[207,208] Nevertheless, COSMO-RS gives consistent predictions for acidities in aqueous and non-aqueous solvents.[209,210] A recent report[13] demonstrated that COSMO-RS can be used to compute solvation free energies in different sol-

vent and reagent mixtures and COSMO-RS recently outperformed 91 different solvation models in a logP prediction blind challenge for drug-like molecules.[211]

The solvation free energy calculated with COSMO-RS is used to connect the gas-phase reaction free energy to the solution-phase reaction free energy as shown in Scheme 3.1.

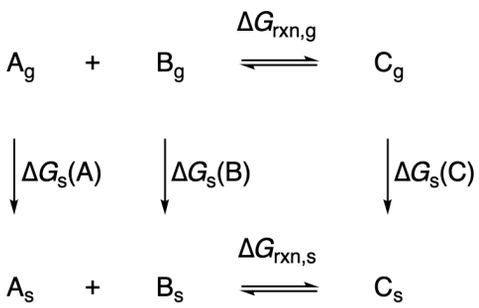

Scheme 3.1. Thermodynamic cycle of COSMO-RS calculations for reaction free energies in the condensed-phase. ΔG_s(i) is the solvation free energy of the given component.

The energy components in the thermodynamic cycle in Scheme 3.1, *i.e.*, reaction free energy in gas-phase and solvation free energy, can be computed at different levels of theory.[158] Typically, the gas-phase reaction free energy is calculated at the highest level of theory feasible whereas even semi-empirical methods suffice for the solvation free energy. The benefit of this method is that no computationally extensive calculations are required to obtain solvation free energies.

Measurement of acidities or redox potentials of reaction intermediates is often not possible due to their short lifetime and low abundance of the intermediates. Thus, computational prediction can be helpful in assessing these values in non-aqueous environments and the solvation model turns out to be important for both p$K_{a(H)}$ and redox potentials. Systematic computational redox potentials can be achieved using only DCSMs,[124,212] while systematic p$K_{a(H)}$ values can be achieved with theoretical parameters to express pK_a as a function of the reaction energy (ΔE).[213–215]

Eckert and Leito demonstrated that anions with strongly localised charge can be challenging, even for COSMO-RS, when the solvent is weakly stabilising.[210] Nevertheless, the results were consistent for a wide range of localised anions and a systematic (although solvent specific) correction was introduced. Explicit solvent molecules can significantly improve the results by stabilising the localised charge[216,217] but, unfortunately, the performance is not uniform for all solvation models.[218,219] Generally, it is recommended to use the thermodynamic cycle for calculating the condensed phase redox potentials and

acidities,[63,220] where the solvation free energy is calculated with a solvation model such as COSMO-RS.

3.5 Relativistic effects

Relativistic effects become important for molecules where electrons close to the nuclei of certain heavy elements approach the speed of light.[221] As the core electrons of heavy elements approach the speed of light the $1s$ orbital contracts and the effect is transferred to all s and p orbitals in terms of contraction and energetic stabilisation. At the same time, d and f orbitals expand radially and are energetically destabilised.[222] This explains why, for example, mercury is a liquid and gold is yellow while silver is grey. Importantly, relativistic effects explain why gold is a catalyst.

The relativistic contraction of $6s$ and $6p$ orbitals strengthens the gold-ligand bond significantly[223] and creates a low-lying lowest unoccupied molecular orbital (LUMO) in cationic gold. The low-energy LUMO subsequently makes gold a strong Lewis acid.[30] The expansion of the $5d$ orbitals, on the other hand, decreases electron-electron repulsion between the electrons that in turn are held with greater force in the more diffuse orbital.[30] Due to tighter binding of the electrons on the $5d$ orbitals, gold(I) does not undergo oxidative additions.[224]

In this work, the scalar relativistic effects were taken into account by using small-core effective-core potentials (ECP) from the utilised basis sets,[30,196,225–228] which treats the core electrons as a pseudo-potential and only valence electrons are treated separately. In addition to the stabilisation (destabilisation) and contraction (expansion) of orbitals due to the scalar relativistic effects, the $l>0$ orbitals (p, d, f) experience spin-orbit coupling that splits the orbitals to $j = l \pm 1/2$ couples in the fully-relativistic treatment.[221] Pernpointner and Hashmi pointed out that scalar relativistic effects are adequate for gold since spin-orbit coupling does not impact the population or orbital energy levels.[225] For some systems ECPs are able to recover only part of the relativistic effect but benchmark studies show that zeroth-order relativistic approach[229] and ECPs give very similar results.[230] Thus, ECPs were used in this work for treatment of gold.

3.6 Molecular properties

3.6.1 Population analysis

In addition to the above-presented computational methods that are used to calculate reaction (free) energies in this thesis, there are also methods that are used to estimate, for example, charge distributions in the molecule. These include population analysis methods, which correlate with chemical shifts,[16] or partial charges in molecular systems.[231] Although partial charges are not observables, computationally they are expressed as:[150]

$$q_{\mathrm{i}} = Z_{\mathrm{i}} - N(\mathrm{i}) \tag{3.4}$$

where Z_i is the atomic number of atom i and $N(\mathrm{i})$ is the number of electrons associated with atom i. The most widely used method is the Mulliken[232] population analysis that is easy to compute and to interpret, but the results can be heavily affected by the choice of the basis-set.[150] In this work, we have used natural population analysis (NPA)[233,234] – or natural bonding orbital (NBO) – to analyse the partial charges. The NBO analysis suffers from fewer problems compared to Mulliken charges and computing NBO charges is more trivial than computing transition state free energy barriers. In addition, our group has earlier successfully predicted regioselectivity in Pauson-Khand reactions with NBO charges.[15,16] In Publication I and section 4.2.1, we found that NBO charges accurately predicted TS barriers and stabilities of intermediates for aldehyde mediated ynone transposition.

3.6.2 Reactivity indices

Nucleophilicity and electrophilicity of molecules help organic chemists to rationalise reactivity and selectivity between reagents and to understand functional group tolerance. The Hammett equation[235] and the empirical substituent – or σ – constants are routinely used to estimate electron-donating or electron-withdrawing effects of functional groups and how they change the rates and equilibria of organic reactions.[236] In essence, the substituent constants can be used to describe the relative nucleophilicity and electrophilicity of similar molecules. While the substituent constants are readily available for *meta*- and *para*-positions of the benzene ring the effect of *ortho*-substituents, however, cannot be determined with the Hammett equation since they introduce additional steric effects. In Publication I, we experienced this short-coming when we were unable to rationalise the reactivity differences between, for ex-

ample, *para*-anisaldehyde, asaronaldehyde, and pivaladehyde, which inspired us to look beyond the Hammett equation.

An alternative approach is to quantify the electrophilicity and nucleophilicity of the molecule directly. Mayr and coworkers were the first to establish experimental nucleophilicity and electrophilicity scales by measuring reaction rates of bimolecular reactions as a function of electrophilicity and nucleophilicity and connecting the rate constants with the reactivity parameters as[237]

$$\log(k_{20\,^\circ\mathrm{C}}) = s(N + E) \tag{3.5}$$

where $k_{20\,^\circ\mathrm{C}}$ is the bimolecular rate constant; s is the nucleophile-specific slope; N is the nucleophilicity parameter; and E is the electrophilicity parameter. To date, Mayr has published s, N, and E values for over 1200 nucleophiles and 300 electrophiles and collected them in a database with estimations of their reliability.[238] Unfortunately, experimental measurement of nucleophilicity or electrophilicity is still time consuming and can require specialised equipment in addition to the difficulty of measuring short-lived nucleophiles and electrophiles such as free radicals.

Thus, it is of interest to use computational approaches for the estimation of nucleophilicity and electrophilicity. Most notable examples include Parr's global electrophilicity index[239] $\omega = \mu^2/\eta$ (μ is the electronic chemical potential and η is the chemical hardness) and Fukui function[240–242] where local nucleophilicity or electrophilicity are computed from differences in electron density between reference state and one-electron oxidised or reduced states, respectively. The electronic chemical potential and the chemical hardness are calculated from the HOMO-LUMO energies,[243] and the global electrophilicity index has many alternative presentations[244] as well as global nucleophilicity index variants,[245,246] ω^-. It must be noted that while different expressions for ω and ω^- give good correlation with experimental values, the biggest shortcoming is that no universal solution has yet been found for either index. Alternative, empirical approaches include using tetracyanoethylene[247] as the reference nucleophile for nucleophilicity, or the methyl anion[248] to correlate electrophilicities of different neutral molecules and cations.

Recently, Pratihar studied the correlation of computational global electrophilicities and nucleophilicities with experimentally measured electrophilicities and nucleophilicities for (hetero)aryls[245] and aldehydes[246] and found excellent correlations. In Publication I, we utilised the global nucleophilicity descriptor that Pratihar demonstrated to give the most consistent results for aldehydes.[246] For further details, see Publication I.

3.7 Reaction kinetics

In situ reaction monitoring is a powerful experimental tool that offers valuable information on the reaction progress from relative assessment of reaction rate coefficients to partial orders of reagents. The kinetic analysis can guide computational inspection of the mechanism as well as further experiments. Together they help to assess the likelihood of different mechanistic proposals, as was done in Publication I. The recent developments in kinetic analysis have been possible due to advances in reaction monitoring technology, especially the development of two new analysis methods in the past two decades.

Firstly, the reaction progress kinetic analysis (RPKA),[18,19] developed by Blackmond uses rate profiles from isothermal calorimetry for reaction monitoring. The rate data should be validated with an orthogonal technique such as FTIR (Fourier transformed infrared) spectroscopy, where the reagent concentrations are measured as a function of time, to ascertain that the rate profiles belong to the desired reaction.[18] The obtained rate *versus* time profile can be converted to conversion *versus* time when necessary and, for analysis of partial orders, the RPKA method utilises reaction rate *versus* substrate concentration data.

Secondly, the variable time normalization analysis (VTNA),[20,21] developed by Burés uses the directly measured conversion reaction profiles from, for example, NMR or FTIR spectroscopy. Conversion of concentration to rate *versus* time data, however, requires a non-trivial integration of the measured data and always involves a line-fitting process, which can cause significant noise in the integrated results. Hence it is not recommended for carrying out the conversion and, in VTNA, the partial orders are defined from the concentration *versus* time profiles.

Both contemporary methods – RPKA and VTNA – streamline the data collection and analysis of reaction profiles and partial orders, as well as rate constants. Contrary to classical methods, like the initial rate method, they use the whole reaction profile for the analysis.[249] The methods rely on visual inspection of the measured data: when will two – or more – reaction profiles overlay each other. The overlaying method is used to determine the partial orders of reagents, for example, A and B in Scheme 3.2, as well as catalyst activation, deactivation and inhibition.[250]

Rate-laws for catalytic reactions such as the one presented in Scheme 3.2 can be complicated. They are often expressed as power laws as in equation 3.6:

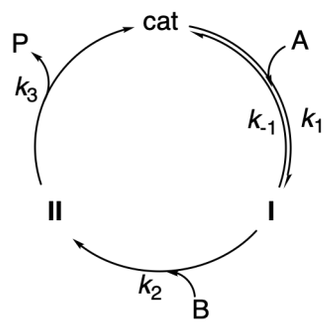

Scheme 3.2. Simplified catalytic cycle for catalytic conversion of **A** + **B** into **P** via intermediates **I** and **II**.

$$rate = -\frac{d[\mathrm{A}]}{dt} = -\frac{d[\mathrm{B}]}{dt} = \frac{d[\mathrm{P}]}{dt} = k[\mathrm{A}]^a[\mathrm{B}]^b[\mathrm{cat}]^\gamma \tag{3.6}$$

Where rate is the macroscopic reaction rate; k is the reaction rate coefficient; [i] is the concentration of reagent i; and the coefficient j in $[\mathrm{i}]^j$ is the partial order of [i]. The partial orders, which are not confined to positive integers, define the molecularity of the reaction's rate-determining step; the resting state of the catalyst; and saturation. The partial orders are an average of the whole reaction unless the analysis is limited to a certain section of the reaction profile.

To solve the partial order of reagent A, for example, with VTNA method, the time integral of $[\mathrm{A}]^a$ is approximated using the trapezoid rule in equation 3.7:

$$\int_0^t [\mathrm{A}]^a dt = \sum_{i=1}^{n} \left(\frac{[\mathrm{A}]_i - [\mathrm{A}]_{i-1}}{2} \right)^a (t_i - t_{i-1}) \tag{3.7}$$

Conversion profiles with different $[\mathrm{A}]_0$ will overlay when the concentrations are raised to the correct power a. Measurement of only two reaction profiles with different initial concentrations for A while concentration of other species are kept the same are enough to determine the partial order a. The normalization is applied independently to all reaction components, including the catalyst, with identical experimentation to determine their partial orders. When the kinetic effect of all components is combined with the reaction profile, all measured reaction profiles should overlap and the slope of the profile is equal to the rate coefficient k in equation 3.6.

The partial order is not necessarily a constant throughout the reaction, but can change as the conditions change.[21,251] It also depends on the initial conditions of the reaction. For example, in the catalytic cycle of Scheme 3.2, the partial order of [A] can vary between 1 and 0 depending on whether the analysis is carried out in diluted or concentrated conditions, respectively.[251]

4. Results

4.1 General

The results of this work are published in three separate peer-reviewed articles and two separate manuscripts listed on page iii, with author contributions on page iv. Here, a short summary is given of the results in Publications I–V. Important parts of the work in Publications II–V were included in the Supplementary Information of the articles and the reader should also refer to them. Small comparison studies were additionally carried out that were not included in the original publications, and they are presented in this Chapter.

All computations were performed with the TURBOMOLE,[252] ORCA,[253] COSMOtherm,[8,9,202] and CREST,[11] programs. The semi-empirical GFN-xTB[10] method was used for crude geometry optimisations and in conformational sampling with CREST. The resolution-of-the-identity approximation for the Coulomb term (RI-J)[254] or the multipole accelerated RI-J[255] were used in this work with the corresponding auxiliary basis sets.[197] The approximations speed up the calculations significantly without a noticeable effect on the accuracy of the results.

4.1.1 Accuracy of the computational method for redox potentials and acidity

To evaluate the performance of our computational methods we compared a small subset of recently published experimental cyclic voltammetry measurements in acetonitrile,[212] as well as experimental $pK_{a(H)}$ values in water and DCM/DCE with corresponding computational E° (equation 2.1) and $pK_{a(H)}$ (equation 2.2) values. The comparison studies were performed with the dispersion corrected PBE0-D3BJ and PW6B95-D3BJ for redox potentials in acetonitrile and acidity in water, whereas TPSS-D3 and PW6B95-D3 were chosen for acidity in DCM/DCE. These functionals were used in Publications I–V because of their robust performance for geometries and ener-

gies.[1,160] The vibrational frequencies were calculated at same level of theory as the geometries and used without scaling. The chemical potentials were calculated using the quasi-RRHO approximation.[182] The Gibbs free energies with the COSMO solvation model (G_{cosmo}) were calculated as $G_{cosmo} = E_{cosmo} + chemical\ potential$, where E_{cosmo} is the energy with COSMO. The Gibbs free energies with COSMO-RS solvation model ($G_{cosmo-rs}$) were calculated as $G_{cosmo-rs} = E_{gas} + chemical\ potential + \Delta G_{solv}$,[158] where E_{gas} is the gas-phase single-point energy, and ΔG_{solv} is the solvation free energy. The COSMO-RS solvation free energies were computed with the COSMOthermX19 program package using the BP_TZVPD_FINE_19.ctd parameter file based on the BP86/def2-TZVPD level of theory.

Overall, the accuracy of the tested methods for redox potentials is very good with slopes close to one, intercepts close to zero, and the R^2s being greater than 0.9825 in all cases, see Scheme 4.1. A small improvement could be achieved with a better description of solvation effects, *i.e.*, with COSMO-RS. However, three outlier molecules[212] were recognised (green tipped triangles in Scheme 4.1).

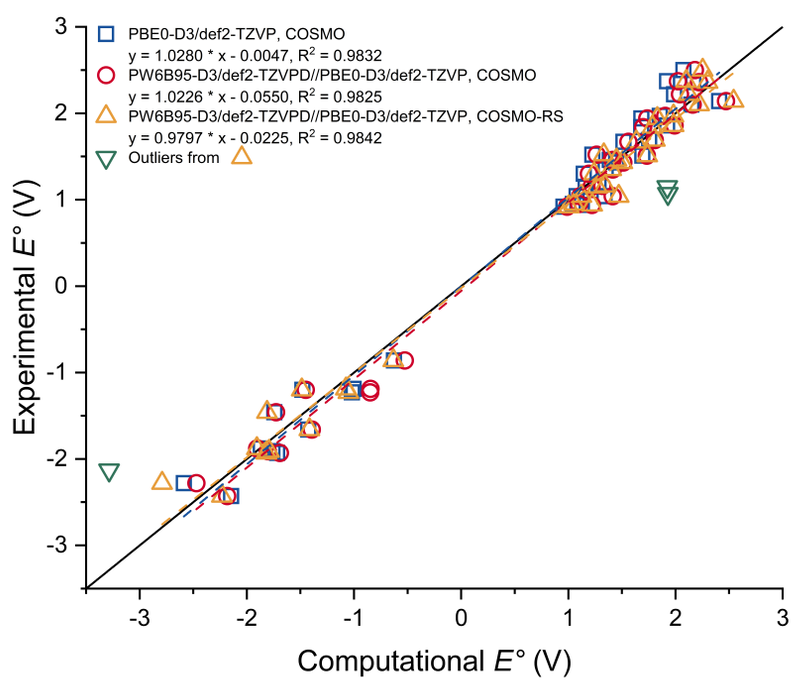

Scheme 4.1. Computational redox potentials (equation 2.1) for a subset of experimentally measured molecules (N=37).[212] The level of theory is indicated in the legend for each data group. Outliers (from left to right): γ-lactone, 2-mercaptobenzoxazole, and imidazole.

Another comparison study was performed to establish the accuracy of our method to calculate $pK_{a(H)}$ values in water and organic solvents. The acidity

of small organic molecules in water, see Scheme 4.2, was affected more by the solvation model than by the choice of functional and basis sets. The COSMO model gave poor performance with the slope being 0.4922 or 0.5330 for PBE0-D3 or PW6B95-D3, respectively, and the accuracy (R^2) being 0.7619 or 0.8222 for PBE0-D3 or PW6B95-D3, respectively. COSMO-RS improves results due to better description of solvent-solute interactions with slope of 0.6974 and R^2= 0.9489 but the acidity of, for example, alcohols is still underestimated. However, Klamt and coworkers have demonstrated that the correct $1/RT\ln(10)$ slope cannot be reproduced even with COSMO-RS and reasoned that the assumed dependence of experimental pK_as on proton dissociation free energies is not correct.[209]

An alternative approach is to compute the proton exchange free energy between a proton acceptor and a proton donor and calculate the p$K_{a(H)}$ as relative to a reference molecule.[218] This approach improves the results significantly due to error cancellation, as is shown in Scheme 4.2. With reference molecules, the results with COSMO became more systematic: R^2 = 0.9326 for PBE0-D3 and R^2 = 0.9376 for PW6B95-D3, but COSMO-RS still gave the best results with R^2 = 0.9706.

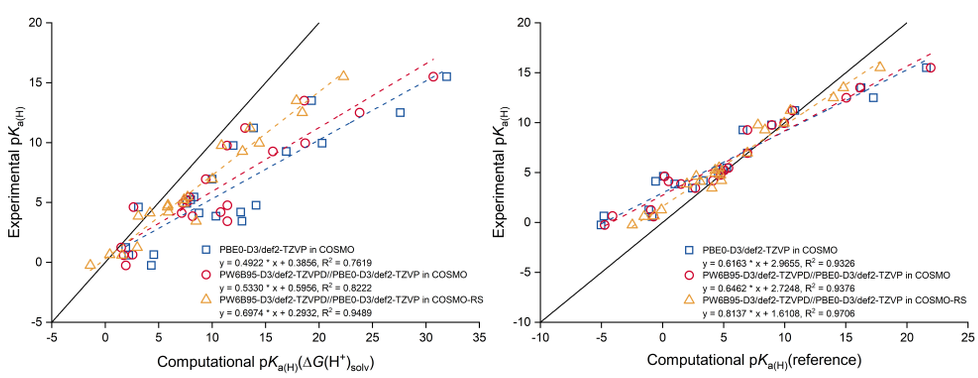

Scheme 4.2. Benchmark of p$K_{a(H)}$ values in water (equation 2.2) for a set of nitrogen bases (N=10) and oxygen acids (N=11). On the left, solvation free energy of a proton in water (-264.0 kcal/mol)[256] is used and, on the right, reference molecules imidazole, acetic acid, and phenol are used to calculate p$K_{a(H)}$ values.

Importantly, the reference molecule has to be similar to the computed molecules. For example, while imidazole (p$K_{a(H)}$ = 6.95) shifted the computed basicities closer to the experimental values, it overestimated the acidity of carboxylic acids and underestimated the acidity of alcohols. Thus, we used acetic acid (pK_a = 4.76) and phenol (pK_a = 9.95) as a reference for carboxylic acids and alcohols (Scheme 4.2), respectively. The acidities of acetic acid and imidazole were then estimated in a 1/4 H_2O:MeOH solvent system according to the study by Rosés[257] and p$K_{a(H)}$-values of the substrates and reagents were calculated

relative to them in Publication II. Imidazole was not measured by Rosés, but we estimated that the behaviour is close to that of the pyridine series.

In Publication V, we needed to accurately describe the pK_a values and solvation of small anions in the non-polar aprotic solvent, DCM. To evaluate our method's performance, we benchmarked experimental acidities in DCE,[258] as the behaviour is similar to DCM.[65] All methods proved to be systematic and, importantly, COSMO-RS systematically improved the acid dissociation free energies, see Scheme 4.3. However, the monoatomic conjugate bases chloride, bromide and iodide required an explicit solvent molecule to stabilise the anion and yield good correlation with the experimental values even with COSMO-RS.

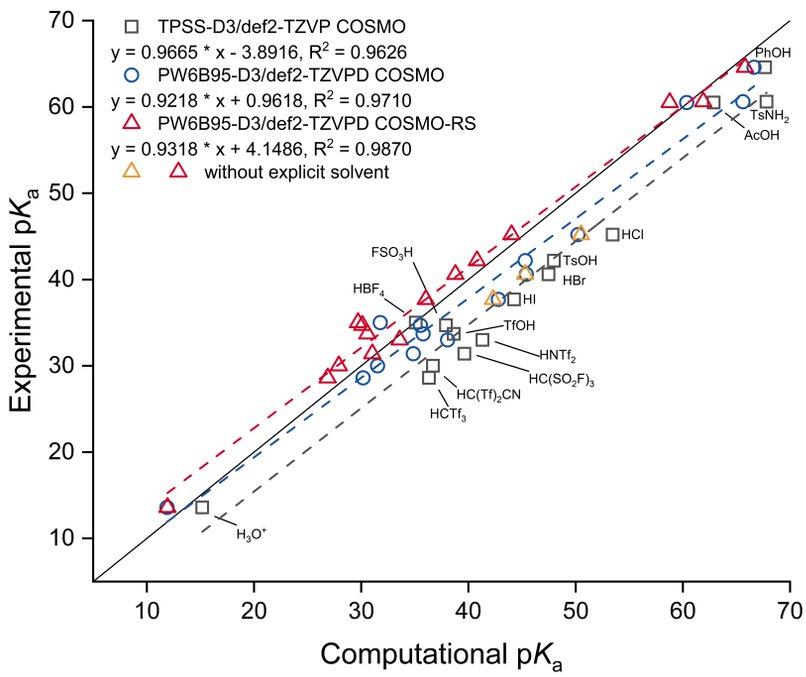

Scheme 4.3. Correlation between experimental and computational pK_a values in DCM/DCE (equation 2.2). The proton free energy of solvation (-207.7 kcal/mol)[258] in DCE was used in the calculation.

4.2 Alkyne activation in homogeneous gold-catalysis

4.2.1 Mechanism of ynone 1,3-*O*-transposition

Ynones are present in natural products and pharmaceuticals and are also utilised as substrates in both TM-catalysed and TM-free synthetic transformations.[259,260] Müller and Segnitz published a platinum catalysed 1,3-*O*-transposition protocol for ynones in 1970[261] and presented the reaction mechanism as an intramolecular transposition, see Scheme 4.4. Over 40 years later, separate studies[22,23] established the gold-catalysed transposition mechanism to proceed via intramolecular oxygen shift based on experimental ^{13}C- and ^{18}O-labelling tests that were supported by computational analysis of the mechanism.[23] Importantly, the transposition is driven by stereoelectronic factors and forms an equilibrium between ynones **22** and **24**.[22]

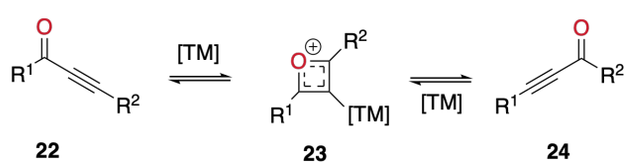

Scheme 4.4. The assumed mechanism for intramolecular 1,3-*O*-transposition.[22,23,261]

However, the activation free energy barrier for the intramolecular transposition in Scheme 4.4 is high in energy – over 27 kcal/mol according to literature reference[23] and our calculations. In the beginning we noticed that this contradicts the experimental conditions: two hours at room temperature with ≥83% yields[22] or 10 minutes at room temperature with ≥42% yields.[23] The expected half-life from the Eyring equation 3.1 for a first-order reaction with 27 kcal/mol activation free energy barrier is 80 days at 298 K. Thus, we investigated the mechanism of gold(I)-catalysed 1,3-*O*-transposition of ynone **25** to **27** more closely (Scheme 4.5).

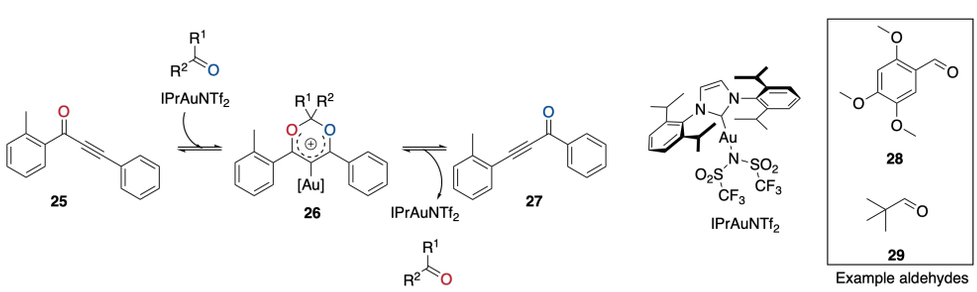

Scheme 4.5. Studied gold(I)-catalysed 1,3-*O*-transposition reaction of ynone **25**.

Computational and kinetic analyses both revealed that the transposition was intermolecular and the substrate mediated the intermolecular transposition more efficiently than the product, which guided further experiments with aldehyde additives. Experimentally, electron-rich aromatic aldehydes, for example **28**, exhibited higher reaction rates while electron deficient aldehydes, for example **29**, inhibited the reaction. The aldehyde **29** formed a stable intermediate $\mathbf{26_{29}}$ that could be characterised in NMR. Formation of the cyclic acetal intermediate with **29** competed with the transposition mediated by **25**/**27** and only partially inhibited the gold-catalyst by forming a stable gold-complex, $\mathbf{26_{29}}$. A further ^{18}O-labelling experiment with **28** verified that the oxygen was transferred from the mediator to the final product.

The inhibiting effect of electron deficient aldehydes, for example, **29**, was explained by a change in the rate-limiting step. Characteristically, the nucleophilic addition was slightly higher for electron deficient aldehydes than for substrate/product-mediated reactions, but the rate-determining step was the acetal cleavage.

Finally, in order to make the reaction more applicable, simplified models are desired as it excludes the need to screen multiple transition states for different substrates in addition to lower computational cost and often higher accuracy.[262,263] The NBO charge located at the carbonyl oxygen correlated with the relative activation free energy barriers for the nucleophilic addition to the gold activated alkyne in Publication I. Later, we noticed that the NBO charges of the carbonyl carbon predicted the stability of the acetal intermediate **30** while the sum of C=O's NBO charges predicted the subsequent activation free energy barrier of the acetal cleavage **31** in Scheme 4.6. However, NBO charges were unable to predict the activation free energy barrier of the rate-determining step for a given aldehyde.

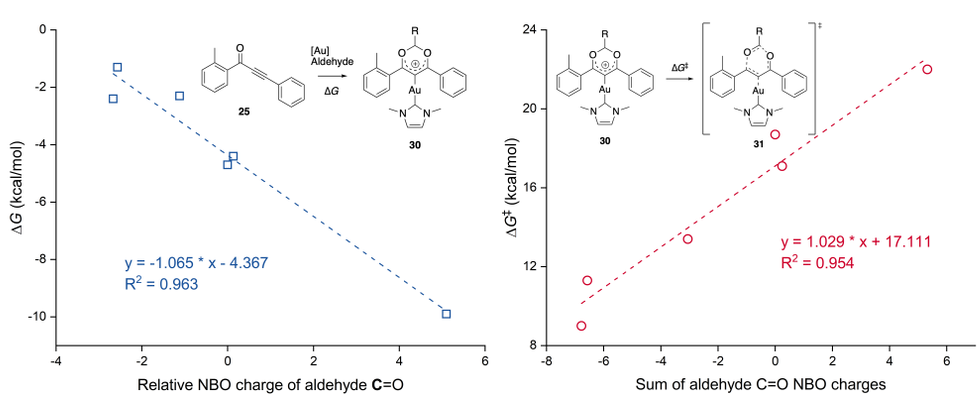

Scheme 4.6. On the left, ΔG of acetal formation *versus* the carbonyl carbon NBO charge normalized to benzaldehyde. On the right, $\Delta G^{\ddagger}$ of acetal cleavage *versus* the sum of C=O NBO charges normalized to benzaldehyde.

We then calculated nucleophilicity factors from HOMO-LUMO energy gaps[246] for the set of studied aldehydes, but found no correlation with activation free energy barriers of the rate-determining step. Visual inspection of the HOMOs showed that electron-rich aldehydes, for example, **28**, had π-type population on the carbonyl oxygen whereas other aldehydes, such as benzaldehyde, had mainly σ-type population on the carbonyl oxygen. When HOMO-n orbitals (n is the number of the HOMO orbital) with π-character on carbonyl oxygen were used instead of strictly using HOMOs the model predicted the activation free energy barrier of the rate-limiting step for the aldehydes.

4.2.2 Design of H-bond donor side-arms for gold-catalysis

Previously, Helaja *et al.*[41] demonstrated that nucleophilic substitution of the chloride anion from gold(III) centre with Lewis basic ligand side-arm can be used to activate the precatalytic gold-chloride salt without silver salts. Stabilisation of the substituted anion was crucial as it was discovered that a hydrogen bond donor solvent or additive, like 1,1,1-trifluoroethanol, improved the catalytic activity.[230] This rationale led us to develop ligand side-arms with hydrogen bond donor functional groups, and to use them in gold catalysis. We selected oxazoline cyclisation in Scheme 4.7 as the benchmark reaction, because the reaction has been widely studied with both Au(I) and Au(III) catalysts.[38,48,49,53,55,264] The ligated gold catalyst **34** with tosyl amide functionalised side-arm gave the best performance in oxazoline synthesis outperforming many commercial catalysts as well as gold-catalysts with loosely bound counterions.

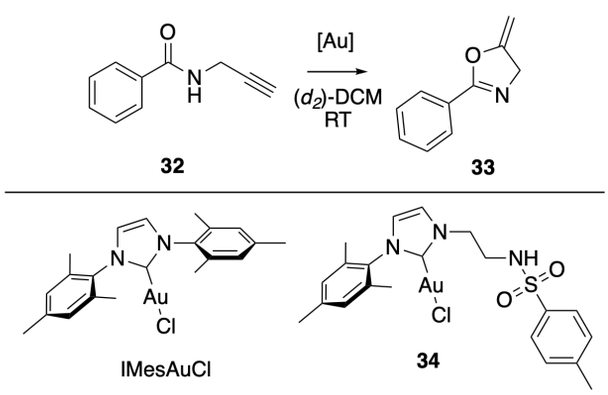

Scheme 4.7. Example of oxazoline cyclization and the compared gold(I)-catalysts.

The catalyst **34** lowered the Au-Cl bond activation free energy barrier compared to the commercial IMesAuCl catalyst, see Scheme 4.8. Comparison of different hydrogen bonding patterns in the substrate addition to gold revealed that H-bond donation from the substrate's NH to the side-arm's sul-

fonyl oxygen in **34-TS1** increased the hydrogen bonding strength between side-arm's NH and chlorine and also lowered the activation free energy barrier, see Scheme 4.8. The conformer **34-TS1'**, where both NHs coordinate to chloride, was close in energy but 0.8 kcal/mol higher.

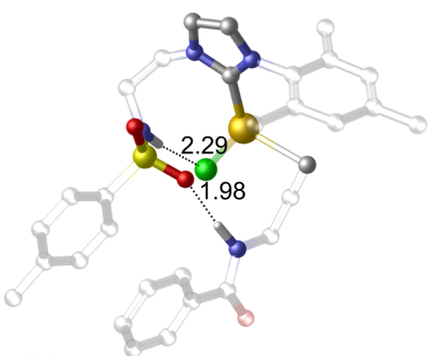

34-TS1
$\Delta G^{\ddagger}$ = 13.2 kcal/mol

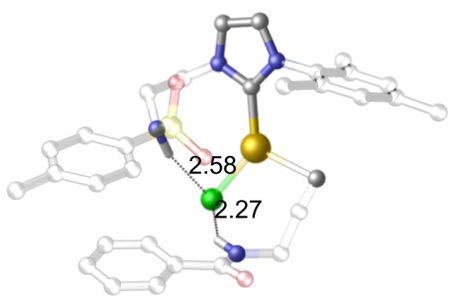

34-TS1'
$\Delta G^{\ddagger}$ = 14.0 kcal/mol

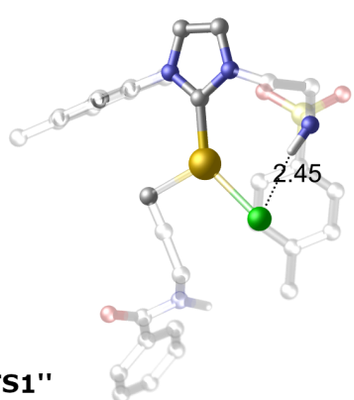

34-TS1''
$\Delta G^{\ddagger}$ = 18.2 kcal/mol

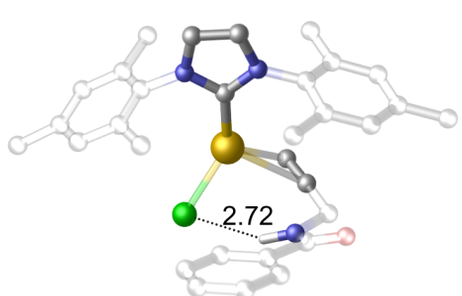

IMesAuCl-**TS1**
$\Delta G^{\ddagger}$ = 16.8 kcal/mol

Scheme 4.8. Hydrogen bonding between chloride, substrate, and tosyl amide functionalised side-arm, with catalysts **34** (top row, and bottom left) and IMesAuCl (bottom right) in substrate addition to gold.

Monodentate hydrogen bond donation to chlorine from the side-arm (**34-TS1"**) or the substrate (IMesAuCl-**TS1**) increased the barrier by 5.0 or 3.6 kcal/mol, respectively, which indicated that two hydrogen bond donors are needed in the activation of the Au-Cl bond. Importantly, in enyne cyclisation, where the substrates did not have any hydrogen bond donor groups, the activation of catalyst **34** necessitated use of acidic hydrogen bond donor additives, for example, 1,1,1-trifluoroacetic acid and *para*-toluenesulfonic acid, while in the presence of non-acidic 1,1,1-trifluoroethanol the catalyst **34** was not activated.

Following the addition, formation of bidentate hydrogen bond donation from the substrate's and **34**'s NHs to the chloride stabilised the activated catalyst intermediate **34-C** by 6.6 kcal/mol compared to the monodentate coordination of the chloride ion in IMesAuCl-**C**, see Scheme 4.9.

34-C
ΔG = 7.9 kcal/mol

IMesAuCl-**C**
ΔG = 14.5 kcal/mol

Scheme 4.9. The bicoordinate complexes for activated **34** (left) and IMesAuCl (right).

In reaction monitoring, it was noted that a small amount of water increased the reaction rate. The rate-determining step was not, however, the Au-Cl bond activation, but the cyclisation or protodeauration. Thus, we inspected how the energy profile of the reaction changed when the chloride a) assisted in the cyclisation and protodeauration, or b) was solvated in the bulk solution by water. In the chloride anion assisted cyclisation **34-TS3**, both substrate and side-arm NH's coordinated to the chloride anion, and the activation free energy barrier was lowered by 5.0 kcal/mol compared to IMesAuCl-**TS3**, Scheme 4.10. Also, when the chloride was solvated out of the system with water, the side-arm's sulfonyl oxygen hydrogen bonded with the substrate's NH in **34-TS3-Cl**$^-$ and lowered the activation free energy barrier by 4.4 kcal/mol compared to IMesAuCl-**TS3-Cl**$^-$, see Scheme 4.10.

Interestingly, the side-arm had a smaller effect in the proton transfer step. The proton was abstracted from the cyclised intermediate by the product molecule[49] and, if the chloride anion is in the system, the role of the side-arm is to stabilise the anion when product **33** replaces it at the hydrogen bonding site of the intermediate. With IMesAuCl, this stabilisation was not possible and thus **TS4** was 6.9 kcal/mol higher in energy compared to **34**. However, if the chloride was solvated by water, the proton abstraction was isoenergetic between **34** and IMesAuCl: $\Delta\Delta G^{\ddagger} = 0.1$ kcal/mol.

In the protodeauration step, the side-arm did not help to stabilise the chlo-

ride anion and both catalysts had similar activation free energy barriers for chloride mediated protodeauration with $\Delta\Delta G^{\ddagger} = 0.3$ kcal/mol. Likewise, when the chloride was solvated by water and the product mediated the protodeauration, the difference between the activation free energy barriers was 1.0 kcal/mol.

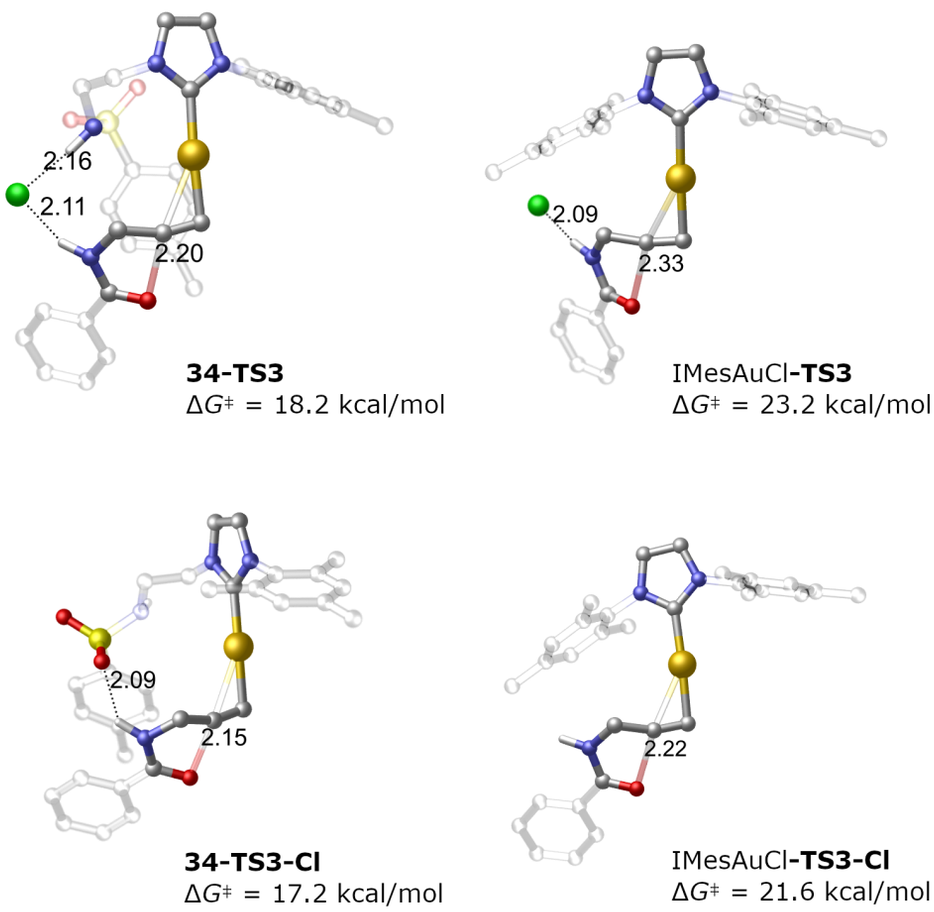

Scheme 4.10. The *5-exo-dig* cyclisation step with **34** (left column) and IMesAuCl (right column) when chloride is in the system (top row) or solvated out (bottom row).

4.3 Photoreduction of nitro heteroarenes

4.3.1 Reaction mechanism of reduction of N-heterocyclic nitro groups to amines

Helaja and co-workers[17] developed a mild *O*-debenzylation method for electron rich N-heterocycles in photoreductive conditions. The authors showed that the reduction potential of the protonated quinoline correlated with the excited state photocatalyst's oxidation potential. Mechanistic investigations supported the sequential proton-electron transfer mechanism because reduction potentials of protonated N-heterocycles could be used to select a sufficiently powerful photocatalyst to reduce the substrate. During the substrate scope study,[17] the authors noticed that when a quinoline with both nitro group and OBn was present, the nitro group was reduced to amine instead of *O*-debenzylation. Because reports of mild photoreductive nitro reductions are scarce, we optimized the reaction conditions in Publication II and studied the mechanism of the photoreductive conversion of nitro heteroarenes to corresponding amines. $Ru(bpy)_3Cl_2$, abbreviated as [Ru^{2+}], was found to be the optimal photocatalyst and ascorbic acid ($AscH_2$) was used as the sacrificial reductant.

We first studied the conversion of nitro quinoline **35** to amine **38** with NMR monitoring, to determine whether the reduction happens via the direct route or condensation mechanism, see Scheme 4.11,[265] but observed no condensation intermediates in the NMR monitoring. Next, to understand the mechanism of nitro and hydroxyl amine reduction steps and the reason why some substrates produced no product or stopped at the hydroxyl amine intermediate, we compared the free energies of different proton-electron transfer steps.

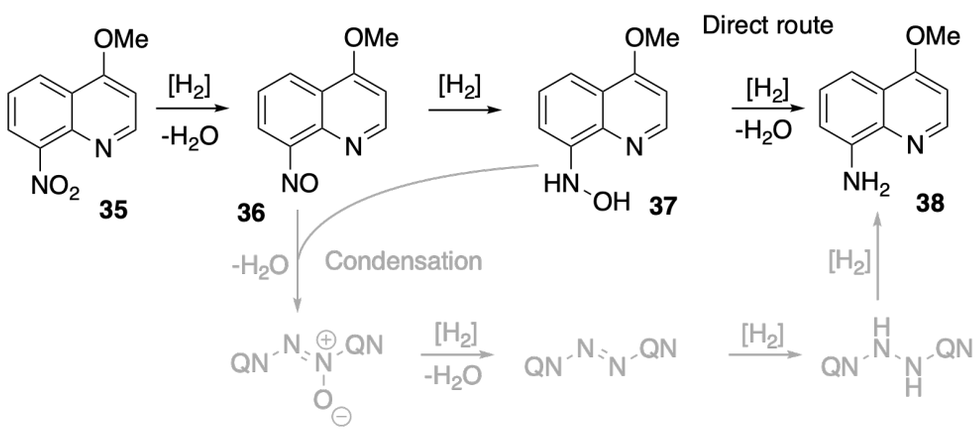

Scheme 4.11. Direct route and condensation mechanism for nitro reduction to amine.[265] Condensation intermediates marked in grey, were not observed.

First, we investigated the reduction potentials of protonated N-heterocycles but found no correlation with the reactivity. However, we noticed that the conjugate acids of the heteroaryls were more acidic than $AscH_2$, which indicated that this is not a viable mechanism. Additionally, oxidation of $AscH_2$ or reduction of non-protonated substrates was not thermodynamically feasible with $^3[*Ru^{2+}]$. The computational results thus indicated, from a thermochemical perspective, that the mechanism is MS-PCET between the $^3[*Ru^{2+}]$, $AscH_2$, and substrate, which was supported by Stern-Volmer measurements.

Later, we examined the computational hydrogen bond complex formation free energies for the same substrates as studied in Publication II. Interestingly, the substrates which yielded (hydroxyl) amine, for example, **40**, had $\Delta G_A \leq 3.4$ kcal/mol, while substrates that did not react, for example, **39**, had $\Delta G_A \geq 5.4$ kcal/mol, see Scheme 4.12. The systematic nature of the results indicates that the nitro quinoline substrates, which produced (hydroxyl) amines hydrogen bonded with $AscH_2$, while the substrates that were unreactive did not hydrogen bond with $AscH_2$. This is in accordance with the prerequisite of PCET reactions.[98] Inspection of the nature of the subsequent quenching with the hydrogen bonded complexes, however, revealed that only the reduction is an exergonic process with $^3[*Ru^{2+}]$ and would thus be the second step in the reaction mechanism. To discern whether the $^3[*Ru^{2+}]$ first oxidises or reduces the $AscH_2$ or substrate, respectively, would require time-resolved emission spectroscopy methods to assess whether the quenching is oxidative or reductive.[96]

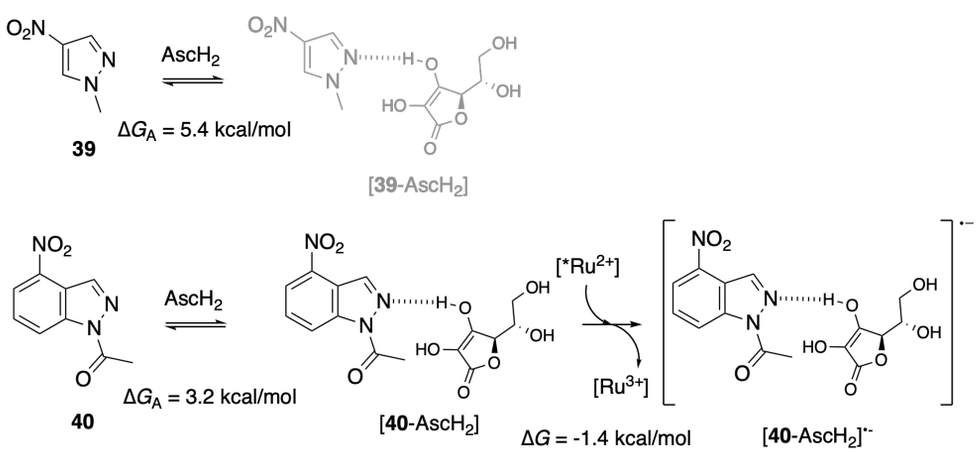

Scheme 4.12. Two examples of hydrogen bonded complexes: **39** is unreactive while **40** yields hydroxyl amine.

The electron rich hydroxyl amine intermediates were more basic and inferior electron acceptors compared to their nitro counterparts, and we noticed that the acidities of the hydroxyl amine N-heterocycles correlated with their

respective reactivities. Thus, we concluded that electron poor quinolines operate *via* MS-PCET mechanism while electron rich quinolines operate *via* the SPET mechanism.

4.4 Oxidative dehydrogenative C-C coupling of aryls

4.4.1 Mechanistic findings from carbocatalysed ODH C-C coupling of (hetero)aryls

Helaja *et al.*[132] had utilised HNO_3-oxidised AC for 3,3'-homocoupling of benzofused heterocycles. We decided to use similar a oxidation procedure for CNTs and extended the scope to include aryl homocoupling products and also intramolecular ODH C-C couplings. In the reaction optimisation, we noticed that the yields were drastically affected by the positioning of functional groups in the *o*-terphenyls **41** and **42** (Scheme 4.13).

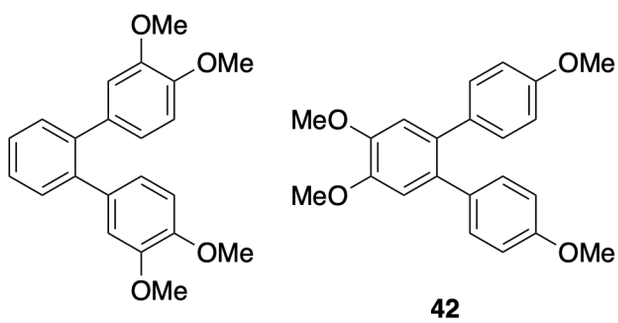

Scheme 4.13. *O*-terphenyls with the yields of cyclized product

The activation free energy barriers for radical cation C-C bond formation were very different: 24.7 kcal/mol and 38.8 kcal/mol for **41** and **42**, respectively. The predicted barrier for **42** would be expected to lead to a kinetically unfeasible reaction and did not explain the observed reactivity. The arenium cation C-C coupling activation free energy barriers, on the other hand, failed to explain the poor reactivity of **42** compared to **41**, as both barriers were close to 27 kcal/mol. Because the thermoneutral analysis[24] failed to explain the relative reactivity, we used the model quinoidic fragments introduced in Scheme 2.8 to take into account the thermodynamics between oxidation and protonation.

The free energy profiles with model quinones revealed that both radical cation and arenium cation C-C bond formations are energetically feasible in the reaction conditions; but to understand the change in operative mechanism, we wanted to comprehend where the difference between the two molecules originated. The methoxy groups in **42** are in a deactivating position relative to the C-C bond forming carbon, while for **41** the net effect is activating.[236] Importantly, the methoxy group promotes protonation at both *ortho*- and *para*-positions of the C-C bond forming carbon in **42**, whereas electron-withdrawing

groups like NO_2 and Br do not and fail to deliver cyclised products in oxidising conditions.[266]

In Publication IV we explored the effect of the carbon material on the product distribution of cascade ODH C-C coupling of various 2,2'-benzofused heterocycles, for example **43** (Table 4.1). The oxidation method – together with the topology – of the parent carbon material drastically affected the product selectivity of the cascade ODH C-C coupling.

Table 4.1: Aryl-aryl coupling reactions with different carbon materials

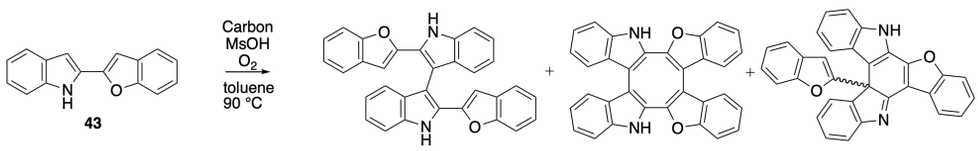

Entry	Carbon (eq.)	MsOH (eq.)	Yield/**44** (%)	Yield/**45** (%)	Yield/**46** (%)
1	oAC-HNO_3 (3)	3	0	0	**79**
2	oAC-air(Δ) (5)	5	0	**58**	0
3	oCNT-HNO_3 (5)	5	24	9	7

Following the findings in Publication III, we investigated the selectivity of the two mechanisms for the ODH C-C coupling reaction of **44**. The radical cation C-C coupling mechanism favoured COT **45** formation, whereas arenium cation C-C bond formation favoured the dearomatized migratory product **46**. By considering the thermodynamics of oxidation and protonation we noticed that AQ as a model quinone favoured protonation and promoted the arenium cation mechanism and product **46**, whereas *o*BQ as a model quinone favoured oxidation and promoted the radical cation mechanism product **45**.

Similar selectivity was found with two oAC catalysts: oAC-HNO_3 was selective for **46** (79%) and oAC-air(Δ) was selective for **45** (58%), see Table 4.1. X-ray photoelectron microscopy revealed that oAC-HNO_3 had significantly more carboxylic groups, whereas the decarboxylated oAC-air(Δ) had more carbonyl and hydroxyl groups. One possible explanation is that the carboxyl groups in oAC-HNO_3 effectively block intermolecular hydrogen bond interactions and thus favour protonation of the substrate molecules by MsOH.[127] Additionally, the lesser amount of intramolecular hydrogen bond donors in oAC-air(Δ) favours intermolecular hydrogen bond interactions with MsOH and consequently favours oxidation of the substrates.[127]

The ODH C-C coupling can happen *via* both radical cation and arenium cation mechanisms. Important factors include the electron and proton affinity of the catalyst and the substrate. Both mechanisms can ultimately yield the same product (Publication III) or lead to different products (Publication IV).

5. Conclusions

In this work, reaction mechanisms were studied with a seamless combination of experimental and computational methods. The combination offered insight of the reaction mechanism that would have not been achieved with experiments or computations alone. The mechanistic understanding was further utilised to describe the reactivity with such concepts as nucleophilicity and acidity to help chemists to utilize the results intuitively for reaction optimisation or design of new catalysts.

In Article I, the reaction mechanism of intermolecular gold(I)-catalysed ynone transposition was comprehensively studied with computations and kinetics. The mechanistic knowledge further guided: trapping of a reaction intermediate; an ^{18}O-labelling experiment; and optimization of the reaction conditions with aldehyde additives to mediate the carbonyl transposition. Based on the combined findings, a simple predictive model was built based on the nucleophilicity of the aldehyde carbonyl oxygen.

In Article V, the activation and utilisation of a new class of gold catalysts with hydrogen bond donor side-arms was designed using a combination of experimental and computational results. The side-arms' role in the gold-chloride bond activation was established from experiments and computations. The side-arms proved to be important in the catalytic cycle by stabilising reaction intermediates and transitions states.

In Article II, the reductive transformation of nitro groups into amines was achieved with photoreductive reaction. The computational results indicated that the first reduction of nitro to nitroso is not sensitive to the basicity of the quinoline, but rather to the hydrogen bonding between quinoline and ascorbic acid. The reduction of hydroxyl amine to the final amine product, on the other hand, does not proceed *via* a hydrogen bonded complex but rather via sequential protonation and reduction of the quinoline.

In Articles III and IV, two competing ODH C-C coupling reaction mechanisms, involving either a radical cation or an arenium cation, were found to be feasible and to coexist for intramolecular C-C bond formations. The

two mechanisms are close in energy and are strongly dependent on the scaling of the activation free energies, *i.e.*, choice of catalyst and substrate. It was found that for aryl-aryl C-C couplings, the nucleophilic carbon centre in the substrate promotes the radical cation mechanism while the less nucleophilic carbon centre promotes the arenium cation mechanism.

Bibliography

[1] L. Goerigk, A. Hansen, C. Bauer, S. Ehrlich, A. Najibi, S. Grimme. A look at the density functional theory zoo with the advanced GMTKN55 database for general main group thermochemistry, kinetics and noncovalent interactions. *Physical Chemistry Chemical Physics* **2017**, *19*, 32184–32215.

[2] S. Miertuš, E. Scrocco, J. Tomasi. Electrostatic interaction of a solute with a continuum. A direct utilizaion of AB initio molecular potentials for the prevision of solvent effects. *Chemical Physics* **1981**, *55*, 117–129.

[3] A. Klamt, G. Schüürmann. COSMO: a new approach to dielectric screening in solvents with explicit expressions for the screening energy and its gradient. *Journal of the Chemical Society, Perkin Transactions 2* **1993**, 799–805.

[4] S. Grimme, J. Antony, S. Ehrlich, H. Krieg. A consistent and accurate ab initio parametrization of density functional dispersion correction (DFT-D) for the 94 elements H-Pu. *The Journal of Chemical Physics* **2010**, *132*, 154104.

[5] S. Grimme, S. Ehrlich, L. Goerigk. Effect of the damping function in dispersion corrected density functional theory. *Journal of Computational Chemistry* **2011**, *32*, 1456–1465.

[6] E. Caldeweyher, C. Bannwarth, S. Grimme. Extension of the D3 dispersion coefficient model. *The Journal of Chemical Physics* **2017**, *147*, 034112.

[7] G. P. Chen, V. K. Voora, M. M. Agee, S. G. Balasubramani, F. Furche. Random-Phase Approximation Methods. *Annual Review of Physical Chemistry* **2017**, *68*, 421–445.

[8] A. Klamt. Conductor-like Screening Model for Real Solvents: A New Approach to the Quantitative Calculation of Solvation Phenomena. *The Journal of Physical Chemistry* **1995**, *99*, 2224–2235.

[9] A. Klamt, V. Jonas, T. Bürger, J. C. W. Lohrenz. Refinement and

Parametrization of COSMO-RS. *The Journal of Physical Chemistry A* **1998**, *102*, 5074–5085.

[10] S. Grimme, C. Bannwarth, P. Shushkov. A Robust and Accurate Tight-Binding Quantum Chemical Method for Structures, Vibrational Frequencies, and Noncovalent Interactions of Large Molecular Systems Parametrized for All spd-Block Elements (Z = 1–86). *Journal of Chemical Theory and Computation* **2017**, *13*, 1989–2009.

[11] P. Pracht, F. Bohle, S. Grimme. Automated exploration of the low-energy chemical space with fast quantum chemical methods. *Physical Chemistry Chemical Physics* **2020**, *22*, 7169–7192.

[12] K. H. Hopmann. How To Make Your Computational Paper Interesting and Have It Published. *Organometallics* **2019**, *38*, 603–605.

[13] M. Muuronen, P. Deglmann, Ž. Tomović. Design Principles for Rational Polyurethane Catalyst Development. *The Journal of Organic Chemistry* **2019**, *84*, 8202–8209.

[14] D. J. Tao, M. Muuronen, Y. Slutskyy, A. Le, F. Furche, L. E. Overman. Diastereoselective Coupling of Chiral Acetonide Trisubstituted Radicals with Alkenes. *Chemistry – A European Journal* **2016**, *22*, 8786–8790.

[15] E. Fager-Jokela, M. Muuronen, M. Patzschke, J. Helaja. Electronic Regioselectivity of Diarylalkynes in Cobalt-Mediated Pauson–Khand Reaction: An Experimental and Computational Study with Para- and Meta-Substituted Diarylalkynes and Norbornene. *The Journal of Organic Chemistry* **2012**, *77*, 9134–9147.

[16] E. Fager-Jokela, M. Muuronen, H. Khaizourane, A. Vázquez-Romero, X. Verdaguer, A. Riera, J. Helaja. Regioselectivity of Intermolecular Pauson–Khand Reaction of Aliphatic Alkynes: Experimental and Theoretical Study of the Effect of Alkyne Polarization. *The Journal of Organic Chemistry* **2014**, *79*, 10999–11010.

[17] A. R. Todorov, T. Wirtanen, J. Helaja. Photoreductive Removal of *O*-Benzyl Groups from Oxyarene N-Heterocycles Assisted by *O*-Pyridine–pyridone Tautomerism. *The Journal of Organic Chemistry* **2017**, *82*, 13756–13767.

[18] D. G. Blackmond. Reaction Progress Kinetic Analysis: A Powerful Methodology for Mechanistic Studies of Complex Catalytic Reactions. *Angewandte Chemie International Edition* **2005**, *44*, 4302–4320.

[19] D. G. Blackmond. Kinetic Profiling of Catalytic Organic Reactions as a Mechanistic Tool. *Journal of the American Chemical Society* **2015**, *137*, 10852–10866.

[20] J. Burés. A Simple Graphical Method to Determine the Order in Catalyst. *Angewandte Chemie International Edition* **2016**, *55*, 2028–2031.

[21] J. Burés. Variable Time Normalization Analysis: General Graphical Elucidation of Reaction Orders from Concentration Profiles. *Angewandte Chemie International Edition* **2016**, *55*, 16084–16087.

[22] R. Kazem Shiroodi, M. Soltani, V. Gevorgyan. Gold-Catalyzed 1,3-Transposition of Ynones. *Journal of the American Chemical Society* **2014**, *136*, 9882–9885.

[23] D.-Y. Li, Y. Wei, M. Shi. Gold(I)-Catalyzed 1,3-*O*-Transposition Reactions: Ynesulfonamides to Ynamides. *European Journal of Organic Chemistry* **2015**, *2015*, 4108–4113.

[24] P. Rempala, J. Kroulík, B. T. King. Investigation of the Mechanism of the Intramolecular Scholl Reaction of Contiguous Phenylbenzenes. *The Journal of Organic Chemistry* **2006**, *71*, 5067–5081.

[25] L. Zhai, R. Shukla, S. H. Wadumethrige, R. Rathore. Probing the Arenium-Ion (ProtonTransfer) versus the Cation-Radical (Electron Transfer) Mechanism of Scholl Reaction Using DDQ as Oxidant. *The Journal of Organic Chemistry* **2010**, *75*, 4748–4760.

[26] A. S. K. Hashmi. Gold-Catalyzed Organic Reactions. *Chemical Reviews* **2007**, *107*, 3180–3211.

[27] A. Fürstner, P. Davies. Catalytic Carbophilic Activation: Catalysis by Platinum and Gold π Acids. *Angewandte Chemie International Edition* **2007**, *46*, 3410–3449.

[28] W. A. Nugent. "Black Swan Events" in Organic Synthesis. *Angewandte Chemie International Edition* **2012**, *51*, 8936–8949.

[29] B. Ranieri, I. Escofet, A. M. Echavarren. Anatomy of gold catalysts: facts and myths. *Organic & Biomolecular Chemistry* **2015**, *13*, 7103–7118.

[30] D. J. Gorin, F. D. Toste. Relativistic effects in homogeneous gold catalysis. *Nature* **2007**, *446*, 395–403.

[31] M. Livendahl, C. Goehry, F. Maseras, A. M. Echavarren. Rationale for the sluggish oxidative addition of aryl halides to Au(I). *Chemical Communications* **2014**, *50*, 1533–1536.

[32] M. Alcarazo, T. Stork, A. Anoop, W. Thiel, A. Fürstner. Steering the Surprisingly Modular π-Acceptor Properties of N-Heterocyclic Carbenes: Implications for Gold Catalysis. *Angewandte Chemie International Edition* **2010**, *49*, 2542–2546.

[33] M. A. Carvajal, J. J. Novoa, S. Alvarez. Choice of Coordination Number

in d^{10} Complexes of Group 11 Metals. *Journal of the American Chemical Society* **2004**, *126*, 1465–1477.

[34] A. Leyva-Pérez, A. Corma. Similarities and Differences between the "Relativistic" Triad Gold, Platinum, and Mercury in Catalysis. *Angewandte Chemie International Edition* **2012**, *51*, 614–635.

[35] D. Wang, R. Cai, S. Sharma, J. Jirak, S. K. Thummanapelli, N. G. Akhmedov, H. Zhang, X. Liu, J. L. Petersen, X. Shi. "Silver Effect" in Gold(I) Catalysis: An Overlooked Important Factor. *Journal of the American Chemical Society* **2012**, *134*, 9012–9019.

[36] M. Wegener, F. Huber, C. Bolli, C. Jenne, S. F. Kirsch. Silver-Free Activation of Ligated Gold(I) Chlorides: The Use of $[Me_3NB_{12}Cl_{11}]-$ as a Weakly Coordinating Anion in Homogeneous Gold Catalysis. *Chemistry – A European Journal* **2015**, *21*, 1328–1336.

[37] J. H. Teles, S. Brode, M. Chabanas. Cationic Gold(I) Complexes: Highly Efficient Catalysts for the Addition of Alcohols to Alkynes. *Angewandte Chemie International Edition* **1998**, *37*, 1415–1418.

[38] A. S. K. Hashmi, J. P. Weyrauch, W. Frey, J. W. Bats. Gold Catalysis: Mild Conditions for the Synthesis of Oxazoles from *N*-Propargylcarboxamides and Mechanistic Aspects. *Organic Letters* **2004**, *6*, 4391–4394.

[39] A. C. Reiersølmoen, D. Csókás, S. Øien Ødegaard, A. Vanderkooy, A. K. Gupta, A.-C. C. Carlsson, A. Orthaber, A. Fiksdahl, I. Pápai, M. Erdélyi. Catalytic Activity of trans-Bis(pyridine)gold Complexes. *Journal of the American Chemical Society* **2020**, *142*, 6439–6446.

[40] M. Pažický, A. Loos, M. J. Ferreira, D. Serra, N. Vinokurov, F. Rominger, C. Jäkel, A. S. K. Hashmi, M. Limbach. Synthesis, Reactivity, and Electrochemical Studies of Gold(I) and Gold(III) Complexes Supported by N-Heterocyclic Carbenes and Their Application in Catalysis. *Organometallics* **2010**, *29*, 4448–4458.

[41] M. Muuronen, J. E. Perea-Buceta, M. Nieger, M. Patzschke, J. Helaja. Cationic Gold Catalysis with Pyridine-Tethered Au(III) NHC-Carbenes: An Experimental and DFT Computational Study. *Organometallics* **2012**, *31*, 4320–4330.

[42] E. Tomás-Mendivil, P. Y. Toullec, J. Borge, S. Conejero, V. Michelet, V. Cadierno. Water-Soluble Gold(I) and Gold(III) Complexes with Sulfonated N-Heterocyclic Carbene Ligands: Synthesis, Characterization, and Application in the Catalytic Cycloisomerization of γ-Alkynoic Acids into Enol-Lactones. *ACS Catalysis* **2013**, *3*, 3086–3098.

[43] E. Tomás-Mendivil, P. Y. Toullec, J. Díez, S. Conejero, V. Michelet, V. Cadierno. Cycloisomerization versus Hydration Reactions in Aqueous Media: A Au(III)-NHC Catalyst That Makes the Difference. *Organic Letters* **2012**, *14*, 2520–2523.

[44] J. C. Timmerman, B. D. Robertson, R. A. Widenhoefer. Gold-Catalyzed Intermolecular Anti-Markovnikov Hydroamination of Alkylidenecyclopropanes. *Angewandte Chemie International Edition* **2015**, *54*, 2251–2254.

[45] A. Couce-Rios, A. Lledós, I. Fernández, G. Ujaque. Origin of the Anti-Markovnikov Hydroamination of Alkenes Catalyzed by L–Au(I) Complexes: Coordination Mode Determines Regioselectivity. *ACS Catalysis* **2019**, *9*, 848–858.

[46] M. Trinchillo, P. Belanzoni, L. Belpassi, L. Biasiolo, V. Busico, A. D'Amora, L. D'Amore, A. Del Zotto, F. Tarantelli, A. Tuzi, D. Zuccaccia. Extensive Experimental and Computational Study of Counterion Effect in the Reaction Mechanism of NHC-Gold(I)-Catalyzed Alkoxylation of Alkynes. *Organometallics* **2016**, *35*, 641–654.

[47] G. Ciancaleoni, L. Belpassi, D. Zuccaccia, F. Tarantelli, P. Belanzoni. Counterion Effect in the Reaction Mechanism of NHC Gold(I)-Catalyzed Alkoxylation of Alkynes: Computational Insight into Experiment. *ACS Catalysis* **2015**, *5*, 803–814.

[48] Z. Lu, J. Han, O. E. Okoromoba, N. Shimizu, H. Amii, C. F. Tormena, G. B. Hammond, B. Xu. Predicting Counterion Effects Using a Gold Affinity Index and a Hydrogen Bonding Basicity Index. *Organic Letters* **2017**, *19*, 5848–5851.

[49] Y. Liu, P. Liu, B. Ling, G. Chen, T. Chen, Y. Li, S. Bi, D. Zhang. Mechanistic Investigation of Au(III)-Catalyzed Cycloisomerizations of *N*-Propargylcarboxamides. *European Journal of Organic Chemistry* **2019**, *2019*, 6822–6829.

[50] R. BabaAhmadi, P. Ghanbari, N. A. Rajabi, A. S. K. Hashmi, B. F. Yates, A. Ariafard. A Theoretical Study on the Protodeauration Step of the Gold(I)-Catalyzed Organic Reactions. *Organometallics* **2015**, *34*, 3186–3195.

[51] M. Chiarucci, M. Bandini. New developments in gold-catalyzed manipulation of inactivated alkenes. *Beilstein Journal of Organic Chemistry* **2013**, *9*, 2586–2614.

[52] C. M. Krauter, A. S. K. Hashmi, M. Pernpointner. A New Insight into Gold(I)-Catalyzed Hydration of Alkynes: Proton Transfer. *Chem-*

CatChem **2010**, *2*, 1226–1230.

[53] L. Biasiolo, A. Del Zotto, D. Zuccaccia. Toward Optimizing the Performance of Homogeneous L-Au-X Catalysts through Appropriate Matching of the Ligand (L) and Counterion ($X^{\smile}$). *Organometallics* **2015**, *34*, 1759–1765.

[54] J. Schießl, J. Schulmeister, A. Doppiu, E. Wörner, M. Rudolph, R. Karch, A. S. K. Hashmi. An Industrial Perspective on Counter Anions in Gold Catalysis: Underestimated with Respect to "Ligand Effects". *Advanced Synthesis & Catalysis* **2018**, *360*, 2493–2502.

[55] W. Wang, G. B. Hammond, B. Xu. Ligand Effects and Ligand Design in Homogeneous Gold(I) Catalysis. *Journal of the American Chemical Society* **2012**, *134*, 5697–5705.

[56] I. Kaljurand, T. Rodima, I. Leito, I. A. Koppel, R. Schwesinger. Self-Consistent Spectrophotometric Basicity Scale in Acetonitrile Covering the Range between Pyridine and DBU. *The Journal of Organic Chemistry* **2000**, *65*, 6202–6208.

[57] M. Namazian, C. Y. Lin, M. L. Coote. Benchmark Calculations of Absolute Reduction Potential of Ferricinium/Ferrocene Couple in Nonaqueous Solutions. *Journal of Chemical Theory and Computation* **2010**, *6*, 2721–2725.

[58] E. Raamat, K. Kaupmees, G. Ovsjannikov, A. Trummal, A. Kütt, J. Saame, I. Koppel, I. Kaljurand, L. Lipping, T. Rodima, V. Pihl, I. A. Koppel, I. Leito. Acidities of strong neutral Brønsted acids in different media. *Journal of Physical Organic Chemistry* **2013**, *26*, 162–170.

[59] J. J. Warren, T. A. Tronic, J. M. Mayer. Thermochemistry of Proton-Coupled Electron Transfer Reagents and its Implications. *Chemical Reviews* **2010**, *110*, 6961–7001.

[60] M. T. Huynh, C. W. Anson, A. C. Cavell, S. S. Stahl, S. Hammes-Schiffer. Quinone 1 e^- and 2 e^-/2 H^+ Reduction Potentials: Identification and Analysis of Deviations from Systematic Scaling Relationships. *Journal of the American Chemical Society* **2016**, *138*, 15903–15910.

[61] G. Gritzner, J. Kuta. Recommendations on reporting electrode potentials in nonaqueous solvents. *Pure and Applied Chemistry* **1983**, *56*, 461–466.

[62] P. Winget, C. J. Cramer, D. G. Truhlar. Computation of equilibrium oxidation and reduction potentials for reversible and dissociative electron-transfer reactions in solution. *Theoretical Chemistry Accounts* **2004**, *112*, 217–227.

[63] J. Ho, M. L. Coote, C. J. Cramer, D. G. Truhlar., *Theoretical calculation*

of reduction potentials, O. Hammerich, B. Speiser (Eds.), CRC Press, **2015**, book section Chapter 6, pp. 1–1685.

[64] A. J. Bard, L. R. Faulkner, *Electrochemical Methods: Fundamentals and Applications*, John Wiley & Sons, **2000**.

[65] A. Kütt, S. Selberg, I. Kaljurand, S. Tshepelevitsh, A. Heering, A. Darnell, K. Kaupmees, M. Piirsalu, I. Leito. pK_a values in organic chemistry – Making maximum use of the available data. *Tetrahedron Letters* **2018**, *59*, 3738–3748.

[66] `https://analytical.chem.ut.ee/databases/pka-values-acids/`.

[67] `https://analytical.chem.ut.ee/databases/pka-values/`.

[68] D. Himmel, S. K. Goll, I. Leito, I. Krossing. Anchor Points for the Unified Brønsted Acidity Scale: The rCCC Model for the Calculation of Standard Gibbs Energies of Proton Solvation in Eleven Representative Liquid Media. *Chemistry – A European Journal* **2011**, *17*, 5808–5826.

[69] C. Reichardt, T. Welton, *Solvents and Solvent Effects in Organic Chemistry 4th ed.*, Wiley-VCH Verlag GmbH & Co. KGaA, **2010**.

[70] A. Kütt, T. Rodima, J. Saame, E. Raamat, V. Mäemets, I. Kaljurand, I. A. Koppel, R. Y. Garlyauskayte, Y. L. Yagupolskii, L. M. Yagupolskii, E. Bernhardt, H. Willner, I. Leito. Equilibrium Acidities of Superacids. *The Journal of Organic Chemistry* **2011**, *76*, 391–395.

[71] K. Abdur-Rashid, T. P. Fong, B. Greaves, D. G. Gusev, J. G. Hinman, S. E. Landau, A. J. Lough, R. H. Morris. An Acidity Scale for Phosphorus-Containing Compounds Including Metal Hydrides and Dihydrogen Complexes in THF: Toward the Unification of Acidity Scales. *Journal of the American Chemical Society* **2000**, *122*, 9155–9171.

[72] J. Saame, T. Rodima, S. Tshepelevitsh, A. Kütt, I. Kaljurand, T. Haljasorg, I. A. Koppel, I. Leito. Experimental Basicities of Superbasic Phosphonium Ylides and Phosphazenes. *The Journal of Organic Chemistry* **2016**, *81*, 7349–7361.

[73] M. A. Ischay, M. E. Anzovino, J. Du, T. P. Yoon. Efficient Visible Light Photocatalysis of [2+2] Enone Cycloadditions. *Journal of the American Chemical Society* **2008**, *130*, 12886–12887.

[74] D. A. Nicewicz, D. W. C. MacMillan. Merging Photoredox Catalysis with Organocatalysis: The Direct Asymmetric Alkylation of Aldehydes. *Science* **2008**, *322*, 77–80.

[75] J. M. R. Narayanam, J. W. Tucker, C. R. J. Stephenson. Electron-Transfer Photoredox Catalysis: Development of a Tin-Free Reductive Dehalogenation Reaction. *Journal of the American Chemical Society*

2009, *131*, 8756–8757.

[76] C. K. Prier, D. A. Rankic, D. W. C. MacMillan. Visible Light Photoredox Catalysis with Transition Metal Complexes: Applications in Organic Synthesis. *Chemical Reviews* **2013**, *113*, 5322–5363.

[77] N. A. Romero, D. A. Nicewicz. Organic Photoredox Catalysis. *Chemical Reviews* **2016**, *116*, 10075–10166.

[78] K. Kalyanasundaram. Photophysics, photochemistry and solar energy conversion with tris(bipyridyl)ruthenium(II) and its analogues. *Coordination Chemistry Reviews* **1982**, *46*, 159–244.

[79] S. Campagna, F. Puntoriero, F. Nastasi, G. Bergamini, V. Balzani, *Photochemistry and Photophysics of Coordination Compounds: Ruthenium*, V. Balzani, S. Campagna (Eds.), Springer Berlin Heidelberg, Berlin, Heidelberg, **2007**, pp. 117–214.

[80] J. K. McCusker. Femtosecond Absorption Spectroscopy of Transition Metal Charge-Transfer Complexes. *Accounts of Chemical Research* **2003**, *36*, 876–887.

[81] N. H. Damrauer, G. Cerullo, A. Yeh, T. R. Boussie, C. V. Shank, J. K. McCusker. Femtosecond Dynamics of Excited-State Evolution in $[Ru(bpy)_3]^{2+}$. *Science* **1997**, *275*, 54–57.

[82] A. Juris, V. Balzani, P. Belser, A. von Zelewsky. Characterization of the Excited State Properties of Some New Photosensitizers of the Ruthenium (Polypyridine) Family. *Helvetica Chimica Acta* **1981**, *64*, 2175–2182.

[83] C. R. Bock, J. A. Connor, A. R. Gutierrez, T. J. Meyer, D. G. Whitten, B. P. Sullivan, J. K. Nagle. Estimation of excited-state redox potentials by electron-transfer quenching. Application of electron-transfer theory to excited-state redox processes. *Journal of the American Chemical Society* **1979**, *101*, 4815–4824.

[84] L. Marzo, S. K. Pagire, O. Reiser, B. König. Visible-Light Photocatalysis: Does It Make a Difference in Organic Synthesis? *Angewandte Chemie International Edition* **2018**, *57*, 10034–10072.

[85] R. A. Marcus. On the Theory of Oxidation-Reduction Reactions Involving Electron Transfer. I. *The Journal of Chemical Physics* **1956**, *24*, 966–978.

[86] R. A. Marcus. On the Theory of Oxidation-Reduction Reactions Involving Electron Transfer. II. Applications to Data on the Rates of Isotopic Exchange Reactions. *The Journal of Chemical Physics* **1957**, *26*, 867–871.

[87] R. A. Marcus. Electron transfer reactions in chemistry. Theory and ex-

periment. *Reviews of Modern Physics* **1993**, *65*, 599–610.

[88] C. D. Clark, M. Z. Hoffman. Effect of solution medium on the rate constants of excited-state electron-transfer quenching reactions of ruthenium(II)-diimine photosensitizers. *Coordination Chemistry Reviews* **1997**, *159*, 359–373.

[89] E. V. Anslyn, D. A. Dougherty, *Modern Physical Organic Chemistry*, University Science, **2006**.

[90] C. Stephenson, T. Yoon, D. W. C. MacMillan, *An Overview of the Physical and Photophysical Properties of [Ru(bpy)3]$^{2+}$*, Wiley-VCH Verlag GmbH & Co. KGaA, **2018**, book section 1, pp. 1–24.

[91] I. Ghosh, R. S. Shaikh, B. König. Sensitization-Initiated Electron Transfer for Photoredox Catalysis. *Angewandte Chemie International Edition* **2017**, *56*, 8544–8549.

[92] M. Marchini, G. Bergamini, P. G. Cozzi, P. Ceroni, V. Balzani. Photoredox Catalysis: The Need to Elucidate the Photochemical Mechanism. *Angewandte Chemie International Edition* **2017**, *56*, 12820–12821.

[93] I. Ghosh, J. I. Bardagi, B. König. Reply to "Photoredox Catalysis: The Need to Elucidate the Photochemical Mechanism". *Angewandte Chemie International Edition* **2017**, *56*, 12822–12824.

[94] D. M. Arias-Rotondo, J. K. McCusker. The photophysics of photoredox catalysis: a roadmap for catalyst design. *Chemical Society Reviews* **2016**, *45*, 5803–5820.

[95] N. Turro, *Modern Molecular Photochemistry*, University Science Books, **1991**.

[96] G. Qiu, R. R. Knowles. Rate–Driving Force Relationships in the Multisite Proton-Coupled Electron Transfer Activation of Ketones. *Journal of the American Chemical Society* **2019**, *141*, 2721–2730.

[97] J. M. Mayer. Proton-Coupled Electron Transfer: A Reaction Chemist's View. *Annual Review of Physical Chemistry* **2004**, *55*, 363–390.

[98] J. M. Mayer, D. A. Hrovat, J. L. Thomas, W. T. Borden. Proton-Coupled Electron Transfer versus Hydrogen Atom Transfer in Benzyl/Toluene, Methoxyl/Methanol, and Phenoxyl/Phenol Self-Exchange Reactions. *Journal of the American Chemical Society* **2002**, *124*, 11142–11147.

[99] J. W. Darcy, B. Koronkiewicz, G. A. Parada, J. M. Mayer. A Continuum of Proton-Coupled Electron Transfer Reactivity. *Accounts of Chemical Research* **2018**, *51*, 2391–2399.

[100] V. R. I. Kaila, G. Hummer. Energetics of Direct and Water-Mediated Proton-Coupled Electron Transfer. *Journal of the American Chemical Society* **2011**, *133*, 19040–19043.

[101] S. Hammes-Schiffer. Proton-coupled electron transfer: classification scheme and guide to theoretical methods. *Energy & Environmental Science* **2012**, *5*, 7696–7703.

[102] J. H. Skone, A. V. Soudackov, S. Hammes-Schiffer. Calculation of Vibronic Couplings for Phenoxyl/Phenol and Benzyl/Toluene Self-Exchange Reactions: Implications for Proton-Coupled Electron Transfer Mechanisms. *Journal of the American Chemical Society* **2006**, *128*, 16655–16663.

[103] A. Sirjoosingh, S. Hammes-Schiffer. Proton-Coupled Electron Transfer versus Hydrogen Atom Transfer: Generation of Charge-Localized Diabatic States. *The Journal of Physical Chemistry A* **2011**, *115*, 2367–2377.

[104] S. Hammes-Schiffer, A. A. Stuchebrukhov. Theory of Coupled Electron and Proton Transfer Reactions. *Chemical Reviews* **2010**, *110*, 6939–6960.

[105] L. Biczók, N. Gupta, H. Linschitz. Coupled Electron-Proton Transfer in Interactions of Triplet C_{60} with Hydrogen-Bonded Phenols: Effects of Solvation, Deuteration, and Redox Potentials. *Journal of the American Chemical Society* **1997**, *119*, 12601–12609.

[106] C. M. Morton, Q. Zhu, H. Ripberger, L. Troian-Gautier, Z. S. D. Toa, R. R. Knowles, E. J. Alexanian. C–H Alkylation *via* Multisite-Proton-Coupled Electron Transfer of an Aliphatic C–H Bond. *Journal of the American Chemical Society* **2019**, *141*, 13253–13260.

[107] T. Meyer, M. Huynh, H. Thorp. The Possible Role of Proton-Coupled Electron Transfer (PCET) in Water Oxidation by Photosystem II. *Angewandte Chemie International Edition* **2007**, *46*, 5284–5304.

[108] V. R. I. Kaila, M. I. Verkhovsky, M. Wikström. Proton-Coupled Electron Transfer in Cytochrome Oxidase. *Chemical Reviews* **2010**, *110*, 7062–7081.

[109] M. H. Shaw, V. W. Shurtleff, J. A. Terrett, J. D. Cuthbertson, D. W. C. MacMillan. Native functionality in triple catalytic cross-coupling: sp^3 C–H bonds as latent nucleophiles. *Science* **2016**, *352*, 1304–1308.

[110] G. J. Choi, Q. Zhu, D. C. Miller, C. J. Gu, R. R. Knowles. Catalytic alkylation of remote C–H bonds enabled by proton-coupled electron transfer. *Nature* **2016**, *539*, 268–271.

[111] D. C. Miller, K. T. Tarantino, R. R. Knowles. Proton-Coupled Electron Transfer in Organic Synthesis: Fundamentals, Applications, and Oppor-

tunities. *Topics in Current Chemistry* **2016**, *374*, 30.

[112] G. J. Choi, R. R. Knowles. Catalytic Alkene Carboaminations Enabled by Oxidative Proton-Coupled Electron Transfer. *Journal of the American Chemical Society* **2015**, *137*, 9226–9229.

[113] K. T. Tarantino, P. Liu, R. R. Knowles. Catalytic Ketyl-Olefin Cyclizations Enabled by Proton-Coupled Electron Transfer. *Journal of the American Chemical Society* **2013**, *135*, 10022–10025.

[114] J. Löwe. *Z. Chemie* **1868**, *4*, 603–604.

[115] M. Grzybowski, K. Skonieczny, H. Butenschön, D. T. Gryko. Comparison of Oxidative Aromatic Coupling and the Scholl Reaction. *Angewandte Chemie International Edition* **2013**, *52*, 9900–9930.

[116] M. Grzybowski, B. Sadowski, H. Butenschön, D. T. Gryko. Synthetic Applications of Oxidative Aromatic Coupling – From Biphenols to Nanographenes. *Angewandte Chemie International Edition* **2020**, *59*, 2998–3027.

[117] Y. Avlasevich, C. Kohl, K. Müllen. Facile synthesis of terrylene and its isomer benzoindenoperylene. *Journal of Materials Chemistry* **2006**, *16*, 1053–1057.

[118] S. Kumar, M. Manickam. Oxidative trimerization of *o*-dialkoxybenzenes to hexaalkoxytriphenylenes: molybdenum(v) chloride as a novel reagent. *Chemical Communications* **1997**, 1615–1666.

[119] S. L. Skraba-Joiner, E. C. McLaughlin, A. Ajaz, R. Thamatam, R. P. Johnson. Scholl Cyclizations of Aryl Naphthalenes: Rearrangement Precedes Cyclization. *The Journal of Organic Chemistry* **2015**, *80*, 9578–9583.

[120] J. Liu, A. Narita, S. Osella, W. Zhang, D. Schollmeyer, D. Beljonne, X. Feng, K. Müllen. Unexpected Scholl Reaction of 6,7,13,14-Tetraarylbenzo[*k*]tetraphene: Selective Formation of Five-Membered Rings in Polycyclic Aromatic Hydrocarbons. *Journal of the American Chemical Society* **2016**, *138*, 2602–2608.

[121] X. Dou, X. Yang, G. J. Bodwell, M. Wagner, V. Enkelmann, K. Müllen. Unexpected Phenyl Group Rearrangement during an Intramolecular Scholl Reaction Leading to an Alkoxy-Substituted Hexa-peri-hexabenzocoronene. *Organic Letters* **2007**, *9*, 2485–2488.

[122] A. Ajaz, E. C. McLaughlin, S. L. Skraba, R. Thamatam, R. P. Johnson. Phenyl Shifts in Substituted Arenes via Ipso Arenium Ions. *The Journal of Organic Chemistry* **2012**, *77*, 9487–9495.

[123] L. Zhai, R. Shukla, R. Rathore. Oxidative C−C Bond Formation (Scholl

Reaction) with DDQ as an Efficient and Easily Recyclable Oxidant. *Organic Letters* **2009**, *11*, 3474–3477.

[124] T. Wirtanen, M. Muuronen, J. Hurmalainen, H. M. Tuononen, M. Nieger, J. Helaja. Intermolecular oxidative dehydrogenative 3,3′-coupling of benzo[*b*]furans and benzo[*b*]thiophenes promoted by DDQ/H^+: total synthesis of shandougenine B. *Organic Chemistry Frontiers* **2016**, *3*, 1738–1745.

[125] D. J. Jones, B. Purushothaman, S. Ji, A. B. Holmes, W. W. H. Wong. Synthesis of electron-poor hexa-peri-hexabenzocoronenes. *Chemical Communications* **2012**, *48*, 8066–8068.

[126] A. K. Turek, D. J. Hardee, A. M. Ullman, D. G. Nocera, E. N. Jacobsen. Activation of Electron-Deficient Quinones through Hydrogen-Bond-Donor-Coupled Electron Transfer. *Angewandte Chemie International Edition* **2016**, *55*, 539–544.

[127] T. Nakayama, N. Okumura, B. Uno. Complementary Effect of Intra- and Intermolecular Hydrogen Bonds on Electron Transfer in β-Hydroxy-Anthraquinone Derivatives. *The Journal of Physical Chemistry B* **2020**, *124*, 848–860.

[128] R. R. S. Shi, M. E. Tessensohn, S. J. L. Lauw, N. A. B. Y. Foo, R. D. Webster. Tuning the reduction potential of quinones by controlling the effects of hydrogen bonding, protonation and proton-coupled electron transfer reactions. *Chemical Communications* **2019**, *55*, 2277–2280.

[129] M. Kamo, A. Tsuda, Y. Nakamura, N. Aratani, K. Furukawa, T. Kato, A. Osuka. Metal-Dependent Regioselective Oxidative Coupling of 5,10,15-Triarylporphyrins with DDQ-$Sc(OTf)_3$ and Formation of an Oxo-quinoidal Porphyrin. *Organic Letters* **2003**, *5*, 2079–2082.

[130] Z.-W. Jiao, Y.-Q. Tu, Q. Zhang, W.-X. Liu, S.-Y. Zhang, S.-H. Wang, F.-M. Zhang, S. Jiang. Tandem C–H oxidation/cyclization/rearrangement and its application to asymmetric syntheses of (–)-brussonol and (–)-przewalskine E. *Nature Communications* **2015**, *6*, 7332.

[131] W. Qi, W. Liu, B. Zhang, X. Gu, X. Guo, D. Su. Oxidative Dehydrogenation on Nanocarbon: Identification and Quantification of Active Sites by Chemical Titration. *Angewandte Chemie International Edition* **2013**, *52*, 14224–14228.

[132] T. Wirtanen, M. K. Mäkelä, J. Sarfraz, P. Ihalainen, S. Hietala, M. Melchionna, J. Helaja. Carbocatalysed Oxidative C_{sp2}-C_{sp2} Homocouplings of Benzo-Fused Heterocycles. *Advanced Synthesis & Catalysis* **2015**, *357*, 3718–3726.

[133] X. Sun, P. Han, B. Li, S. Mao, T. Liu, S. Ali, Z. Lian, D. Su. Oxidative dehydrogenation reaction of short alkanes on nanostructured carbon catalysts: a computational account. *Chemical Communications* **2018**, *54*, 864–875.

[134] O. V. Khavryuchenko, B. Frank, A. Trunschke, K. Hermann, R. Schlögl. Quantum-Chemical Investigation of Hydrocarbon Oxidative Dehydrogenation over Spin-Active Carbon Catalyst Clusters. *The Journal of Physical Chemistry C* **2013**, *117*, 6225–6234.

[135] O. V. Khavryuchenko, B. Frank. Theoretical Investigation of Anion-Radical States of Edge-Oxidized Carbon Model Clusters. *The Journal of Physical Chemistry A* **2017**, *121*, 3167–3173.

[136] O. V. Khavryuchenko, B. Frank. Impact of Edge Oxidation State on Red-Ox Barriers during Hydrocarbon Oxydehydrogenation over Carbon Nanotube Catalysts: A Theoretical Study. *The Journal of Physical Chemistry C* **2017**, *121*, 3958–3962.

[137] M. F. R. Pereira, J. J. M. Órfão, J. L. Figueiredo. Oxidative dehydrogenation of ethylbenzene on activated carbon catalysts. I. Influence of surface chemical groups. *Applied Catalysis A: General* **1999**, *184*, 153–160.

[138] W. Qi, D. Su. Metal-Free Carbon Catalysts for Oxidative Dehydrogenation Reactions. *ACS Catalysis* **2014**, *4*, 3212–3218.

[139] H. Wu, C. Su, R. Tandiana, C. Liu, C. Qiu, Y. Bao, J. Wu, Y. Xu, J. Lu, D. Fan, K. P. Loh. Graphene-Oxide-Catalyzed Direct CH−CH-Type Cross-Coupling: The Intrinsic Catalytic Activities of Zigzag Edges. *Angewandte Chemie International Edition* **2018**, *57*, 10848–10853.

[140] S. Wu, G. Wen, X. Liu, B. Zhong, D. S. Su. Model Molecules with Oxygenated Groups Catalyze the Reduction of Nitrobenzene: Insight into Carbocatalysis. *ChemCatChem* **2014**, *6*, 1558–1561.

[141] S. Wu, G. Wen, J. Wang, J. Rong, B. Zong, R. Schlögl, D. S. Su. Nitrobenzene reduction catalyzed by carbon: does the reaction really belong to carbocatalysis? *Catalysis Science & Technology* **2014**, *4*, 4183–4187.

[142] J. L. Figueiredo, M. F. R. Pereira. The role of surface chemistry in catalysis with carbons. *Catalysis Today* **2010**, *150*, 2–7.

[143] D. G. Truhlar, B. C. Garrett, S. J. Klippenstein. Current Status of Transition-State Theory. *The Journal of Physical Chemistry* **1996**, *100*, 12771–12800.

[144] J. M. Goodman, P. D. Kirby, L. O. Haustedt. Some calculations for

organic chemists: boiling point variation, Boltzmann factors and the Eyring equation. *Tetrahedron Letters* **2000**, *41*, 9879–9882.

[145] F. Jensen, *Introduction to Computational Chemistry 2nd ed.*, John Wiley & Sons, **2013**.

[146] M. Born, K. Huang, *Dynamical theory of crystal lattices*, Oxford UniversityPress, **1954**.

[147] D. R. Hartree. The Wave Mechanics of an Atom with a Non-Coulomb Central Field. Part I. Theory and Methods. *Mathematical Proceedings of the Cambridge Philosophical Society* **1928**, *24*, 89–110.

[148] D. R. Hartree. The Wave Mechanics of an Atom with a Non-Coulomb Central Field. Part II. Some Results and Discussion. *Mathematical Proceedings of the Cambridge Philosophical Society* **1928**, *24*, 111–132.

[149] V. Fock. Näherungsmethode zur Lösung des quantenmechanischen Mehrkörperproblems. *Zeitschrift für Physik* **1930**, *61*, 126–148.

[150] S. M. Bachrach, *Computational Organic Chemistry 2nd ed.*, John Wiley & Sons, **2014**.

[151] P. Hohenberg, W. Kohn. Inhomogeneous Electron Gas. *Physical Review* **1964**, *136*, B864–B871.

[152] W. Kohn, L. J. Sham. Self-Consistent Equations Including Exchange and Correlation Effects. *Physical Review* **1965**, *140*, A1133–A1138.

[153] W. Koch, M. C. Holthausen, *A Chemist's Guide to Density Functional Theory 2nd ed.*, Wiley-VCH Verlag GmbH, **2001**.

[154] D. S. Sholl, J. A. Steckel, *Density Functional Theory: A Practical Introduction*, John Wiley & Sons, **2009**.

[155] D. Rappoport, N. R. M. Crawford, F. Furche, K. Burke, *Approximate Density Functionals: Which Should I Choose?*, R. King, R. Crabtree, C. Lukehart, D. Atwood, R. Scott (Eds.), John Wiley & Sons, **2009**.

[156] A. D. Becke. Density-functional exchange-energy approximation with correct asymptotic behavior. *Physical Review A* **1988**, *38*, 3098–3100.

[157] J. P. Perdew. Density-functional approximation for the correlation energy of the inhomogeneous electron gas. *Physical Review B* **1986**, *33*, 8822–8824.

[158] A. Hellweg, F. Eckert. Brick by brick computation of the Gibbs free energy of reaction in solution using quantum chemistry and COSMO-RS. *AIChE Journal* **2017**, *63*, 3944–3954.

[159] J. Tao, J. P. Perdew, V. N. Staroverov, G. E. Scuseria. Climbing the Density Functional Ladder: Nonempirical Meta–Generalized Gradient

Approximation Designed for Molecules and Solids. *Physical Review Letters* **2003**, *91*, 146401.

[160] L. Goerigk, S. Grimme. A thorough benchmark of density functional methods for general main group thermochemistry, kinetics, and noncovalent interactions. *Physical Chemistry Chemical Physics* **2011**, *13*, 6670–6688.

[161] M. Bühl, H. Kabrede. Geometries of Transition-Metal Complexes from Density-Functional Theory. *Journal of Chemical Theory and Computation* **2006**, *2*, 1282–1290.

[162] M. P. Waller, H. Braun, N. Hojdis, M. Bühl. Geometries of Second-Row Transition-Metal Complexes from Density-Functional Theory. *Journal of Chemical Theory and Computation* **2007**, *3*, 2234–2242.

[163] M. Bühl, C. Reimann, D. A. Pantazis, T. Bredow, F. Neese. Geometries of Third-Row Transition-Metal Complexes from Density-Functional Theory. *Journal of Chemical Theory and Computation* **2008**, *4*, 1449–1459.

[164] F. Furche, J. P. Perdew. The performance of semilocal and hybrid density functionals in $3d$ transition-metal chemistry. *The Journal of Chemical Physics* **2006**, *124*, 044103.

[165] P. Nava, D. Hagebaum-Reignier, S. Humbel. Bonding of Gold with Unsaturated Species. *ChemPhysChem* **2012**, *13*, 2090–2096.

[166] R. Kang, H. Chen, S. Shaik, J. Yao. Assessment of Theoretical Methods for Complexes of Gold(I) and Gold(III) with Unsaturated Aliphatic Hydrocarbon: Which Density Functional Should We Choose? *Journal of Chemical Theory and Computation* **2011**, *7*, 4002–4011.

[167] B. Braïda, P. C. Hiberty, A. Savin. A Systematic Failing of Current Density Functionals: Overestimation of Two-Center Three-Electron Bonding Energies. *The Journal of Physical Chemistry A* **1998**, *102*, 7872–7877.

[168] V. Hrouda, M. Roeselová, T. Bally. The $C_4H_4^{\bullet+}$ Potential Energy Surface. 3. The Reaction of Acetylene with Its Radical Cation. *The Journal of Physical Chemistry A* **1997**, *101*, 3925–3935.

[169] T. Bally, G. N. Sastry. Incorrect Dissociation Behavior of Radical Ions in Density Functional Calculations. *The Journal of Physical Chemistry A* **1997**, *101*, 7923–7925.

[170] A. D. Becke. Density-functional thermochemistry. III. The role of exact exchange. *The Journal of Chemical Physics* **1993**, *98*, 5648–5652.

[171] A. D. Becke. A new mixing of Hartree-Fock and local density-functional theories. *The Journal of Chemical Physics* **1993**, *98*, 1372–1377.

[172] C. Lee, W. Yang, R. G. Parr. Development of the Colle-Salvetti correlation-energy formula into a functional of the electron density. *Physical Review B* **1988**, *37*, 785–789.

[173] C. Adamo, V. Barone. Toward reliable density functional methods without adjustable parameters: The PBE0 model. *The Journal of Chemical Physics* **1999**, *110*, 6158–6170.

[174] Y. Zhao, D. G. Truhlar. Design of Density Functionals That Are Broadly Accurate for Thermochemistry, Thermochemical Kinetics, and Nonbonded Interactions. *The Journal of Physical Chemistry A* **2005**, *109*, 5656–5667.

[175] S. F. Sousa, P. A. Fernandes, M. J. Ramos. General Performance of Density Functionals. *The Journal of Physical Chemistry A* **2007**, *111*, 10439–10452.

[176] S. Grimme. Semiempirical hybrid density functional with perturbative second-order correlation. *The Journal of Chemical Physics* **2006**, *124*, 034108.

[177] I. M. Alecu, J. Zheng, Y. Zhao, D. G. Truhlar. Computational Thermochemistry: Scale Factor Databases and Scale Factors for Vibrational Frequencies Obtained from Electronic Model Chemistries. *Journal of Chemical Theory and Computation* **2010**, *6*, 2872–2887.

[178] H. Ryu, J. Park, H. K. Kim, J. Y. Park, S.-T. Kim, M.-H. Baik. Pitfalls in Computational Modeling of Chemical Reactions and How To Avoid Them. *Organometallics* **2018**, *37*, 3228–3239.

[179] R. F. Ribeiro, A. V. Marenich, C. J. Cramer, D. G. Truhlar. Use of Solution-Phase Vibrational Frequencies in Continuum Models for the Free Energy of Solvation. *The Journal of Physical Chemistry B* **2011**, *115*, 14556–14562.

[180] Y. Zhao, D. G. Truhlar. Computational characterization and modeling of buckyball tweezers: density functional study of concave-convex $\pi \cdots \pi$ interactions. *Physical Chemistry Chemical Physics* **2008**, *10*, 2813–2818.

[181] Y.-P. Li, J. Gomes, S. Mallikarjun Sharada, A. T. Bell, M. Head-Gordon. Improved Force-Field Parameters for QM/MM Simulations of the Energies of Adsorption for Molecules in Zeolites and a Free Rotor Correction to the Rigid Rotor Harmonic Oscillator Model for Adsorption Enthalpies. *The Journal of Physical Chemistry C* **2015**, *119*, 1840–1850.

[182] S. Grimme. Supramolecular Binding Thermodynamics by Dispersion-Corrected Density Functional Theory. *Chemistry – A European Journal* **2012**, *18*, 9955–9964.

[183] A. V. Brethomé, S. P. Fletcher, R. S. Paton. Conformational Effects on Physical-Organic Descriptors: The Case of Sterimol Steric Parameters. *ACS Catalysis* **2019**, *9*, 2313–2323.

[184] S. Riniker, G. A. Landrum. Better Informed Distance Geometry: Using What We Know To Improve Conformation Generation. *Journal of Chemical Information and Modeling* **2015**, *55*, 2562–2574.

[185] P. C. St. John, Y. Guan, Y. Kim, S. Kim, R. S. Paton. Prediction of organic homolytic bond dissociation enthalpies at near chemical accuracy with sub-second computational cost. *Nature Communications* **2020**, *11*, 2328.

[186] A. J. Cohen, P. Mori-Sánchez, W. Yang. Insights into Current Limitations of Density Functional Theory. *Science* **2008**, *321*, 792–794.

[187] A. J. Cohen, P. Mori-Sánchez, W. Yang. Challenges for Density Functional Theory. *Chemical Reviews* **2012**, *112*, 289–320.

[188] J. Oxgaard, O. Wiest. Symmetry, Radical Ions, and Butadienes: Exploring the Limits of Density Functional Theory. *The Journal of Physical Chemistry A* **2001**, *105*, 8236–8240.

[189] S. Grimme, R. Huenerbein, S. Ehrlich. On the Importance of the Dispersion Energy for the Thermodynamic Stability of Molecules. *ChemPhysChem* **2011**, *12*, 1258–1261.

[190] J. Klimeš, A. Michaelides. Perspective: Advances and challenges in treating van der Waals dispersion forces in density functional theory. *The Journal of Chemical Physics* **2012**, *137*, 120901.

[191] S. Grimme. Density functional theory with London dispersion corrections. *WIREs Computational Molecular Science* **2011**, *1*, 211–228.

[192] J.-D. Chai, M. Head-Gordon. Long-range corrected hybrid density functionals with damped atom–atom dispersion corrections. *Physical Chemistry Chemical Physics* **2008**, *10*, 6615–6620.

[193] J. G. Hill. Gaussian basis sets for molecular applications. *International Journal of Quantum Chemistry* **2013**, *113*, 21–34.

[194] F. Jensen. Atomic orbital basis sets. *WIREs Computational Molecular Science* **2013**, *3*, 273–295.

[195] F. Weigend, F. Furche, R. Ahlrichs. Gaussian basis sets of quadruple zeta valence quality for atoms H–Kr. *The Journal of Chemical Physics* **2003**, *119*, 12753–12762.

[196] F. Weigend, R. Ahlrichs. Balanced basis sets of split valence, triple zeta valence and quadruple zeta valence quality for H to Rn: Design and

assessment of accuracy. *Physical Chemistry Chemical Physics* **2005**, *7*, 3297–3305.

[197] F. Weigend. Accurate Coulomb-fitting basis sets for H to Rn. *Physical Chemistry Chemical Physics* **2006**, *8*, 1057–1065.

[198] D. Rappoport, F. Furche. Property-optimized Gaussian basis sets for molecular response calculations. *The Journal of Chemical Physics* **2010**, *133*, 134105.

[199] J. Andzelm, C. Kölmel, A. Klamt. Incorporation of solvent effects into density functional calculations of molecular energies and geometries. *The Journal of Chemical Physics* **1995**, *103*, 9312–9320.

[200] V. Barone, M. Cossi, J. Tomasi. Geometry optimization of molecular structures in solution by the polarizable continuum model. *Journal of Computational Chemistry* **1998**, *19*, 404–417.

[201] A. Schäfer, A. Klamt, D. Sattel, J. C. W. Lohrenz, F. Eckert. COSMO Implementation in TURBOMOLE: Extension of an efficient quantum chemical code towards liquid systems. *Physical Chemistry Chemical Physics* **2000**, *2*, 2187–2193.

[202] F. Eckert, A. Klamt. Fast solvent screening via quantum chemistry: COSMO-RS approach. *AIChE Journal* **2002**, *48*, 369–385.

[203] A. Klamt. The COSMO and COSMO-RS solvation models. *WIREs Computational Molecular Science* **2018**, *8*, e1338.

[204] S.-T. Lin, S. I. Sandler. *A Priori* Phase Equilibrium Prediction from a Segment Contribution Solvation Model. *Industrial & Engineering Chemistry Research* **2002**, *41*, 899–913.

[205] A. V. Marenich, C. J. Cramer, D. G. Truhlar. Universal Solvation Model Based on Solute Electron Density and on a Continuum Model of the Solvent Defined by the Bulk Dielectric Constant and Atomic Surface Tensions. *The Journal of Physical Chemistry B* **2009**, *113*, 6378–6396.

[206] S. Tshepelevitsh, M. Oss, A. Pung, I. Leito. Evaluating the COSMO-RS Method for Modeling Hydrogen Bonding in Solution. *ChemPhysChem* **2013**, *14*, 1909–1919.

[207] A. Klamt, J. Reinisch, F. Eckert, A. Hellweg, M. Diedenhofen. Polarization charge densities provide a predictive quantification of hydrogen bond energies. *Physical Chemistry Chemical Physics* **2012**, *14*, 955–963.

[208] A. Klamt, J. Reinisch, F. Eckert, J. Graton, J.-Y. Le Questel. Interpretation of experimental hydrogen-bond enthalpies and entropies from COSMO polarisation charge densities. *Physical Chemistry Chemical Physics* **2013**, *15*, 7147–7154.

[209] A. Klamt, F. Eckert, M. Diedenhofen, M. E. Beck. First Principles Calculations of Aqueous pK_a Values for Organic and Inorganic Acids Using COSMO−RS Reveal an Inconsistency in the Slope of the pKa Scale. *The Journal of Physical Chemistry A* **2003**, *107*, 9380–9386.

[210] F. Eckert, I. Leito, I. Kaljurand, A. Kütt, A. Klamt, M. Diedenhofen. Prediction of acidity in acetonitrile solution with COSMO-RS. *Journal of Computational Chemistry* **2009**, *30*, 799–810.

[211] C. Loschen, J. Reinisch, A. Klamt. COSMO-RS based predictions for the SAMPL6 logP challenge. *Journal of Computer-Aided Molecular Design* **2020**, *34*, 385–392.

[212] H. G. Roth, N. A. Romero, D. A. Nicewicz. Experimental and Calculated Electrochemical Potentials of Common Organic Molecules for Applications to Single-Electron Redox Chemistry. *Synlett* **2016**, *27*, 714–723.

[213] S. Zhang, J. Baker, P. Pulay. A Reliable and Efficient First Principles-Based Method for Predicting pK_a Values. 1. Methodology. *The Journal of Physical Chemistry A* **2010**, *114*, 425–431.

[214] S. Zhang, J. Baker, P. Pulay. A Reliable and Efficient First Principles-Based Method for Predicting pK_a Values. 2. Organic Acids. *The Journal of Physical Chemistry A* **2010**, *114*, 432–442.

[215] K. R. Adam. New Density Functional and Atoms in Molecules Method of Computing Relative pK_a Values in Solution. *The Journal of Physical Chemistry A* **2002**, *106*, 11963–11972.

[216] J. R. Pliego, J. M. Riveros. The Cluster-Continuum Model for the Calculation of the Solvation Free Energy of Ionic Species. *The Journal of Physical Chemistry A* **2001**, *105*, 7241–7247.

[217] J. R. Pliego, J. M. Riveros. Theoretical Calculation of pK_a Using the Cluster-Continuum Model. *The Journal of Physical Chemistry A* **2002**, *106*, 7434–7439.

[218] J. Ho, M. L. Coote. A universal approach for continuum solvent pK_a calculations: are we there yet? *Theoretical Chemistry Accounts* **2009**, *125*, 3.

[219] C. P. Kelly, C. J. Cramer, D. G. Truhlar. Adding Explicit Solvent Molecules to Continuum Solvent Calculations for the Calculation of Aqueous Acid Dissociation Constants. *The Journal of Physical Chemistry A* **2006**, *110*, 2493–2499.

[220] J. Ho, M. L. Coote. First-principles prediction of acidities in the gas and solution phase. *WIREs Computational Molecular Science* **2011**, *1*, 649–660.

[221] P. Pyykkö. Relativistic Effects in Chemistry: More Common Than You Thought. *Annual Review of Physical Chemistry* **2012**, *63*, 45–64.

[222] P. Pyykkö. Relativistic effects in structural chemistry. *Chemical Reviews* **1988**, *88*, 563–594.

[223] J. P. Desclaux, P. Pyykkö. Dirac-Fock one-centre calculations. The molecules CuH, AgH and AuH including p-type symmetry functions. *Chemical Physics Letters* **1976**, *39*, 300–303.

[224] W. Nakanishi, M. Yamanaka, E. Nakamura. Reactivity and Stability of Organocopper(I), Silver(I), and Gold(I) Ate Compounds and Their Trivalent Derivatives. *Journal of the American Chemical Society* **2005**, *127*, 1446–1453.

[225] M. Pernpointner, A. S. K. Hashmi. Fully Relativistic, Comparative Investigation of Gold and Platinum Alkyne Complexes of Relevance for the Catalysis of Nucleophilic Additions to Alkynes. *Journal of Chemical Theory and Computation* **2009**, *5*, 2717–2725.

[226] P. Pyykkö, J. P. Desclaux. Relativity and the periodic system of elements. *Accounts of Chemical Research* **1979**, *12*, 276–281.

[227] M. Lein, M. Rudolph, A. S. K. Hashmi, P. Schwerdtfeger. Homogeneous Gold Catalysis: Mechanism and Relativistic Effects of the Addition of Water to Propyne. *Organometallics* **2010**, *29*, 2206–2210.

[228] D. Andrae, U. Häußermann, M. Dolg, H. Stoll, H. Preuß. Energy-adjusted *ab initio* pseudopotentials for the second and third row transition elements. *Theoretica chimica acta* **1990**, *77*, 123–141.

[229] C. v. Wüllen. Molecular density functional calculations in the regular relativistic approximation: Method, application to coinage metal diatomics, hydrides, fluorides and chlorides, and comparison with first-order relativistic calculations. *The Journal of Chemical Physics* **1998**, *109*, 392–399.

[230] M. Muuronen, *Activation of π-systems in Lewis acid mediated homogenous catalysis*, Thesis, University of Helsinki, **2015**.

[231] C. A. Morales-Rivera, P. E. Floreancig, P. Liu. Predictive Model for Oxidative C–H Bond Functionalization Reactivity with 2,3-Dichloro-5,6-dicyano-1,4-benzoquinone. *Journal of the American Chemical Society* **2017**, *139*, 17935–17944.

[232] R. S. Mulliken. Electronic Population Analysis on LCAO–MO Molecular Wave Functions. I. *The Journal of Chemical Physics* **1955**, *23*, 1833–1840.

[233] A. E. Reed, R. B. Weinstock, F. Weinhold. Natural population analysis.

The Journal of Chemical Physics **1985**, *83*, 735–746.

[234] E. D. Glendening, C. R. Landis, F. Weinhold. Natural bond orbital methods. *WIREs Computational Molecular Science* **2012**, *2*, 1–42.

[235] L. P. Hammett. The Effect of Structure upon the Reactions of Organic Compounds. Benzene Derivatives. *Journal of the American Chemical Society* **1937**, *59*, 96–103.

[236] C. Hansch, A. Leo, R. W. Taft. A survey of Hammett substituent constants and resonance and field parameters. *Chemical Reviews* **1991**, *91*, 165–195.

[237] H. Mayr, A. R. Ofial. Do general nucleophilicity scales exist? *Journal of Physical Organic Chemistry* **2008**, *21*, 584–595.

[238] `https://www.cup.lmu.de/oc/mayr/reaktionsdatenbank2/`.

[239] R. G. Parr, L. v. Szentpály, S. Liu. Electrophilicity Index. *Journal of the American Chemical Society* **1999**, *121*, 1922–1924.

[240] K. Fukui, T. Yonezawa, H. Shingu. A Molecular Orbital Theory of Reactivity in Aromatic Hydrocarbons. *The Journal of Chemical Physics* **1952**, *20*, 722–725.

[241] K. Fukui. Role of Frontier Orbitals in Chemical Reactions. *Science* **1982**, *218*, 747–754.

[242] R. G. Parr, W. Yang. Density functional approach to the frontier-electron theory of chemical reactivity. *Journal of the American Chemical Society* **1984**, *106*, 4049–4050.

[243] T. Koopmans. Über die Zuordnung von Wellenfunktionen und Eigenwerten zu den Einzelnen Elektronen Eines Atoms. *Physica* **1934**, *1*, 104–113.

[244] P. K. Chattaraj, S. Giri, S. Duley. Update 2 of: Electrophilicity Index. *Chemical Reviews* **2011**, *111*, PR43–PR75.

[245] S. Pratihar, S. Roy. Nucleophilicity and Site Selectivity of Commonly Used Arenes and Heteroarenes. *The Journal of Organic Chemistry* **2010**, *75*, 4957–4963.

[246] S. Pratihar. Electrophilicity and nucleophilicity of commonly used aldehydes. *Organic & Biomolecular Chemistry* **2014**, *12*, 5781–5788.

[247] L. R. Domingo, E. Chamorro, P. Pérez. Understanding the Reactivity of Captodative Ethylenes in Polar Cycloaddition Reactions. A Theoretical Study. *The Journal of Organic Chemistry* **2008**, *73*, 4615–4624.

[248] H. Mayr, J. Ammer, M. Baidya, B. Maji, T. A. Nigst, A. R. Ofial, T. Singer. Scales of Lewis Basicities toward C-Centered Lewis Acids

(Carbocations). *Journal of the American Chemical Society* **2015**, *137*, 2580–2599.

[249] C. D. T. Nielsen, J. Burés. Visual kinetic analysis. *Chemical Science* **2019**, *10*, 348–353.

[250] A. Martínez-Carrión, M. G. Howlett, C. Alamillo-Ferrer, A. D. Clayton, R. A. Bourne, A. Codina, A. Vidal-Ferran, R. W. Adams, J. Burés. Kinetic Treatments for Catalyst Activation and Deactivation Processes based on Variable Time Normalization Analysis. *Angewandte Chemie International Edition* **2019**, *58*, 10189–10193.

[251] J. Burés. What is the Order of a Reaction? *Topics in Catalysis* **2017**, *60*, 631–633.

[252] F. Furche, R. Ahlrichs, C. Hättig, W. Klopper, M. Sierka, F. Weigend. Turbomole. *WIREs Computational Molecular Science* **2014**, *4*, 91–100.

[253] F. Neese. Software update: the ORCA program system, version 4.0. *WIREs Computational Molecular Science* **2018**, *8*, e1327.

[254] K. Eichkorn, O. Treutler, H. Öhm, M. Häser, R. Ahlrichs. Auxiliary basis sets to approximate Coulomb potentials. *Chemical Physics Letters* **1995**, *240*, 283–290.

[255] M. Sierka, A. Hogekamp, R. Ahlrichs. Fast evaluation of the Coulomb potential for electron densities using multipole accelerated resolution of identity approximation. *The Journal of Chemical Physics* **2003**, *118*, 9136–9148.

[256] D. Himmel, V. Radtke, B. Butschke, I. Krossing. Basic Remarks on Acidity. *Angewandte Chemie International Edition* **2018**, *57*, 4386–4411.

[257] F. Rived, I. Canals, E. Bosch, M. Rosés. Acidity in methanol–water. *Analytica Chimica Acta* **2001**, *439*, 315–333.

[258] E. Paenurk, K. Kaupmees, D. Himmel, A. Kütt, I. Kaljurand, I. A. Koppel, I. Krossing, I. Leito. A unified view to Brønsted acidity scales: do we need solvated protons? *Chemical Science* **2017**, *8*, 6964–6973.

[259] R. E. Whittaker, A. Dermenci, G. Dong. Synthesis of Ynones and Recent Application in Transition-Metal-Catalyzed Reactions. *Synthesis* **2016**, *48*, 161–183.

[260] C. Nájera, L. K. Sydnes, M. Yus. Conjugated Ynones in Organic Synthesis. *Chemical Reviews* **2019**, *119*, 11110–11244.

[261] E. Müller, A. Segnitz. Eine neue Umlagerungsreaktion von α,α'-Bisacetylen-ketonen. *Synthesis* **1970**, *1970*, 147–149.

[262] C. Sandford, L. R. Fries, T. E. Ball, S. D. Minteer, M. S. Sigman. Mecha-

nistic Studies into the Oxidative Addition of Co(I) Complexes: Combining Electroanalytical Techniques with Parameterization. *Journal of the American Chemical Society* **2019**, *141*, 18877–18889.

[263] J. P. Reid, R. S. J. Proctor, M. S. Sigman, R. J. Phipps. Predictive Multivariate Linear Regression Analysis Guides Successful Catalytic Enantioselective Minisci Reactions of Diazines. *Journal of the American Chemical Society* **2019**, *141*, 19178–19185.

[264] A. S. K. Hashmi. Gold-catalyzed synthesis of N,O-heterocycles. *Pure and Applied Chemistry* **2010**, *82*, 657–668.

[265] F. Haber. Über Galvanisch gefälltes Eisen. *Zeitschrift für Elektrochemie* **1898**, *4*, 410–413.

[266] B. T. King, J. Kroulík, C. R. Robertson, P. Rempala, C. L. Hilton, J. D. Korinek, L. M. Gortari. Controlling the Scholl Reaction. *The Journal of Organic Chemistry* **2007**, *72*, 2279–2288.

Appendix

I. S. Aikonen, M. Muuronen, T. Wirtanen, S. Heikkinen, J. Musgreave, J. Burés, J. Helaja, *ACS Catalysis* **2018**, *8*, 960–967.

II. A. R. Todorov, S. Aikonen, M. Muuronen, J. Helaja, *Organic Letters* **2019**, *21*, 3764–3768; with Pages S32–S36 of the Supplementary Information.

III. T. Wirtanen, S. Aikonen, M. Muuronen, M. Melchionna, M. Kemell, F. Davodi, T. Kallio, T. Hu, J. Helaja, *Chemistry – A European Journal* **2019**, *25*, 12288–12293; with Pages 1–6 of the Supplementary Information.

IV. D. S. Casadio, S. Aikonen, A. Lenarda, M. Nieger, T. Hu, S. Taubert, D. Sundholm, M. Muuronen, T. Wirtanen, J. Helaja, *Manuscript*; with Pages S1–S7 of the Supplementary Information.

V. O. Seppänen, S. Aikonen, M. Muuronen, C. Alamillo-Ferrer, J. Burés, J. Helaja, *Manuscript*; with Pages S1–S10 of the Supplementary Information.